CLOUD TYPES AND THE TROPICAL EARTH RADIATION BUDGET

Harbans L. Dhuria
University of the District of Columbia
Washington, DC 20004

H. Lee Kyle
NASA/Goddard Space Flight Center
Greenbelt, MD 20771

NAG5-1012

Journal of Climate (JCL053)
Submitted April 1989
Revised December 1989

ABSTRACT

Nimbus-7 cloud and Earth radiation budget data are compared in a study of the effects of clouds on the tropical radiation budget. The data consist of daily averages over fixed $(500\ km)^2$ target areas, and the months of July 1979 and January 1980 were chosen to show the effect of seasonal changes. Six climate regions, consisting of 14 to 24 target areas each, were picked for intensive analysis because they exemplified the range in the tropical cloud/net radiation interactions. The normal analysis was to consider net radiation as the independent variable and examine how cloud cover, cloud type, albedo and emitted radiation varied with the net radiation. Two recurring themes keep repeating on a local, regional, and zonal basis: the net radiation is strongly influenced by the average cloud type and amount present, but most net radiation values could be produced by several combinations of cloud types and amount.

The regions of highest net radiation (greater than 125 W/m^2) tend to have medium to heavy cloud cover. In these cases, thin medium altitude clouds predominate. Their cloud tops are normally too warm to be classified as cirrus by the Nimbus cloud algorithm. A common feature in the tropical oceans are large regions where the total regional cloud cover varies from 20% to 90%, but with little regional difference in the net radiation. The monsoon and rain areas are high net radiation regions. The deep convective storm centers tend to have low, often highly negative, net radiation, but these are surrounded by large areas of high net radiation covered by thin medium and high level clouds. Large regional differences in the net radiation caused by varying cloud cover and type do, however, occur in the tropical oceans. The most noticeable difference is between continental land and ocean regions. The

net radiation is considerably higher over the oceans. The largest longitudinal variations in net radiation in July and January occur in high solar insolation regions somewhat poleward of the subsolar point. Over the oceans, net radiation maxima are associated with an average cloud cover of thin mid-altitude clouds, while minima are associated with bright low-altitude clouds. The largest differences, over 100 W/m^2 are between the ocean maxima and the deep minima over the continental deserts. Over the deserts during the summer, however, cloud variations appear less important than regional variations in the surface albedo.

1. INTRODUCTION

The Nimbus-7 Earth Radiation Budget (ERB) and cloud data sets are compared in the tropics for the months of July 1979 and January 1980 to study the effect of clouds on the tropical radiation budget. A knowledge of the effects of clouds on the Earth's radiation budget is important both for accurate medium-range weather forecasting (Slingo, 1987) and for studying possible climate change. General circulation models (GCMs) are the basic tools used in these studies, but the accuracy of their predictions depends on the validity of the physics equations and parameters used. A weak point, at present, is the way GCMs treat clouds. Cess and Potter (1987) compared the estimates of the effects of clouds on the radiative budget as determined by six different general circulation models (GCM's) and found a considerable lack of agreement. Each model incorporated a unique set of model physics and numerical configuration. The problem is complex both because of the multiple effects clouds can have and because in the past there was a scarcity of reliable global observations.

It has been proposed (Platt, 1981) that tropical cirrus clouds tend to increase net radiation (absorbed minus emitted) while the presence of deep convective or low clouds (Hartmann and Short, 1980) will decrease the net radiation. Recent studies by Ardanuy et al. (1989a) and Ramanathan et al. (1989) indicate that clouds do decrease the absorbed net radiation on a global scale. However, regionally the decrease is most prominent at high latitudes in the summer hemisphere. There, optically thick and relatively low cloud fields sharply increase the albedo while only moderately decreasing the outgoing longwave radiation (OLR). In the tropical rain belt, the high cloud tops tend to be both bright and cold. In the mean, the increase in the albedo

caused by these clouds tends to be balanced by the decrease in the OLR. The problem of the overall effect of clouds on the radiation budget comes down to an examination of cloud types and cloud climatological statistics.

The availability of new global data sets such as the Nimbus-7 ERB (Jacobowitz et al., 1984) and cloud (Hwang et al., 1988) results allow a better look both at the complexity of the problem and at global statistics. Some of our colleagues (Ardanuy et al., 1989a,b) are using the two data sets to examine the global statistics. They use an analysis scheme which compares clear-sky and average (all) sky radiance fields. Ramanathan et al. (1989) also studied the problem by comparing clear-sky and all-sky radiances. The latter group used data from the new Earth Radiation Budget Experiment (Barkstrom et al., 1989).

In this paper we restrict ourselves to a comparative study of the complex interaction between clouds and net radiation in the tropics. We do not consider a clear-sky case, but rather consider various types of clouds and varying amounts of cloud cover. Our purpose is to illustrate the wide range of interactions between clouds and the radiation budget that occur in the tropics. Our general approach and analysis scheme will be outlined in Section 2. Data characteristics and sources are discussed in Section 3. The reader is warned that there is some confusion concerning clouds. An aircraft pilot and a theoretical modeler tend to think about and discuss clouds in somewhat different ways and terminologies. Further, a ground observer, an aircraft pilot, and a satellite sensor often make distinctly different observations of the same cloud field. This problem is discussed in Section 3. An overview of the Earth's net radiation budget and cloud fields (60°N to 60°S) is given for July 1979 and January 1980 in Section 4 with emphasis on the tropics. For six

tropical and subtropical study regions, the relationship between cloud cover, cloud type and net, top-of-the-atmosphere radiation is analyzed for the months of July 1979 and January 1980 in Section 5. The general variations in the relationship in the tropics are discussed in Section 6, while conclusions and discussion appear in Section 7.

2. ANALYSIS SCHEME

In this study, we use a comparative procedure to examine how the regional radiation budget varies with changing cloud amount and cloud type. Emphasis is given to how changes in the cloud cover effect the net radiation. In remote sensing experiments the net radiation is determined by the equation:

$$NR = SI - (SW + LW) \tag{1}$$

where:

NR = net radiation

SI = solar insolation (diurnal average)

LW = diurnally averaged OLR

SW = diurnally averaged reflected shortwave (solar) radiation

The measured quantities are SI, LW, and SW. Physically, of course, the net radiation is as real a quantity as any of the others. In fact, we will find in Sections 4 and 5 that many combinations of cloud amount and type, and hence of SW and LW, can produce the same net radiation. To emphasize this fact, we will commonly use the net radiation as the "independent" variable in plotting regional results.

In the Nimbus ERB data set, the diurnally averaged albedo, A, is given instead of SW. The relationship is:

$$SW = A \bullet SI \tag{2}$$

We therefore can transform Eq.(1) to the form:

$$(A \bullet SI + LW) = SI - NR \tag{3}$$

Much of our analysis of regional data will be based on Eq.(3).

The Nimbus ERB and cloud data we use come in the form of daily and monthly averages over a global grid of roughly equal area, $(500\ km)^2$, regions called target areas (TAs). The two data sets were formed from simultaneous measurements from instruments on the Nimbus-7 satellite. From the ERB data set come diurnally averaged albedo, outgoing longwave, and net radiation. From the cloud data set we use both day and night values of the percentage of the target area that is covered by clouds whose tops can be classified as high, middle, or low. The sum of the high, middle, and low clouds gives the total cloud fraction. More details concerning these two data sets are given in Section 3.

Using monthly averages, the characteristics of the net radiation and total cloud fields are examined for July 1979 and January 1980, in Section 4. Particular emphasis is placed on the tropics. Six regions (see Figure 5) are designated for more detailed study in Section 5. A given study region contains 14 to 23 target areas whose monthly means indicate similar total cloud cover and net radiation. Four ocean and two land regions are included.

For each study region the daily data for a given month are reviewed to see how albedo, OLR and net radiation vary with total cloud cover and with cloud type. After rejecting days in which some of the Earth radiation budget or cloud parameters are missing, the study regions have 300 to 430 target area days of data per month.

3. DATA SOURCES

General descriptions of the Nimbus-7 data sets used are given for the Earth radiation budget by Kyle et al. (1985) and for the clouds by Hwang et al. (1988). Daily estimates of fractional clear, low ((0 to 2 km), mid (2 to 7 km), and high (above 7 km) altitude cloud cover near noon and midnight for fixed $(500\ km)^2$ target areas are available. There are 2070 target areas (TA) which cover the globe. A special "cold and dim" subset of the mid and high altitude daytime clouds are termed cirrus clouds. A second, "cold and very bright", subset of the daytime high altitude clouds are called deep convective. We will follow the terminology of Stowe et al., (1988, 1989) and the reader is warned that in this paper the terms cirrus and deep convective have the definitions given above. The clouds in question may or may not be called cirrus or deep convective by a ground or aircraft observer. The ERB scanner data are available on the same $(500\ km)^2$ TA basis, and the observations were taken within minutes of the cloud measurements. The ERB products include noon and midnight outgoing longwave radiation (OLR) measurements and daily averaged values of the albedo, OLR, and net radiation.

During daylight hours, the Nimbus-7 cloud identification scheme uses a bispectral algorithm utilizing 11.5 μm radiances from the Temperature Humidity Infrared Radiometer (THIR) and 0.37 μm reflectivities from the Total Ozone

Mapping Spectrometer (TOMS) both on the Nimbus-7 satellite. In the dark, only the 11.5 μm radiances are available. Stowe et al. (1988) report that the 0.37 μm reflectivities are chiefly used to identify low clouds with little thermal contrast with the surface. At nadir, the footprint sizes are, respectively, $(6\ km)^2$, $(50\ km)^2$, and $(90\ km)^2$ for the THIR, TOMS, and ERB scanners. The THIR 11.5 μm channel, thus, has the best resolution and should do the best job of resolving cloudy and clear regions. Each of its measurements does, however, integrate radiances over an area of 36 km^2 or larger. Because of the lack of fine detail in the measurements, some scientists (see for instance Susskind et al., 1987) use the term "effective cloud fraction" for the retrieved clouds. Both the cloud fraction and the 11.5 μm radiance associated with the cloud top are given. From the blackbody temperature derived from the 11.5 μm radiance, an "effective" cloud top altitude can be derived from regional climatological lapse rates. Only the general altitude descriptors of low, medium, and high are given in the data set. For broken or very thin clouds, the "effective" cloud top will be somewhat lower than the physical cloud top.

There are some difficulties involved with constructing cloud climatologies for general use. Scientists trying to incorporate cloud algorithms in GCMs want, for the radiative transfer routines, information on global and regional cloud amount, mean albedo, ice/water phase, and cloud top and bottom temperatures and emissivities. In addition, latent heat release, rainfall rates, and cloud layer information are important. To date, no climatology covers all of these features, and even the mean global cloud cover is not well established (see Stowe et al., 1989). Traditional cloud atlases classify clouds by their visible, to the human eye, characteristics (see for instance WMO, 1969). These classifications are related to various weather situations but give, at

best, only qualitative information concerning the physical cloud properties modelers now desire. Only satellite sensors can yield consistent, continuous maps of global cloud cover. The Nimbus-7 cloud data set and the International Satellite Cloud Climatology Project (ISCCP) (Schiffer and Rossow, 1983) are two such data sets. However, these data sets also fail to yield much of the desired information. In particular, only the cloud tops are observed and there is no information concerning cloud bases and multiple cloud layers. In addition, present satellite data sets are neither entirely consistent with one another (see for instance Stowe et al., 1989) nor with ground-based observations (Henderson-Sellers et al., 1987).

Fortunately, in our present study we do not need most of the information desired by weather and climate modelers. Our purpose is to examine how top of the atmosphere regional radiation budgets vary with changing cloud cover. To some extent, this can be examined using only the Earth radiation budget albedo and OLR measurements. This was the procedure followed by Ramanathan et al. (1989) in their cloud radiative forcing study. However, the addition of concurrent cloud estimates to the study adds more quantitative information concerning cloud types and amounts and how they affect the albedo and OLR.

The Earth radiation budget products are derived from the Nimbus-7 ERB scanner measurements (Jacobowitz et al., 1984). Kyle et al. (1985, 1986) report some problems with the original products. The scanner longwave fluxes are about 3 W/m^2 too low due to an error in a calibration coefficient, while the albedos are about 12% (three and one-half albedo units) too high, apparently due to the difficulty in differentiating between clear and cloudy scenes (Arking and Vemury, 1984). These errors were verified both from internal evidence and through comparison with both the ERB wide field of view measurements and with

the new Earth Radiation Budget Experiment (ERBE) results (Barkstrom et al., 1989). These latter two results agree fairly well on the global means (Kyle et al., 1990). The errors in the ERB scanner longwave and albedo products oppose each other thus reducing the resultant error in the net radiation. The global mean annual value for the net radiation is -3.2 W/m^2 compared to a preliminary estimate of about +5 W/m^2 from the new ERBE products. However, the best theoretical value for the annual average energy gain is zero, therefore, Barkstrom et al. list their probable error at about ± 5 W/m^2. Thus, despite the errors in the Nimbus-7 scanner shortwave and longwave products, the derived net radiation appears quite reasonable.

The Nimbus ERB Processing Team is reprocessing the scanner data to correct the known defects in the longwave and albedo products (Groveman et al., 1988). A procedure similar to that discussed in Arking and Vemury (1984) has been used to produce monthly averaged target area values of the albedo, OLR, and net radiation. The radiances are sorted by their satellite zenith angle and the viewing azimuth angle and then are converted to fluxes by direct numerical integration. This method is named the Sorting into Angular Bins (SAB) algorithm. The SAB mean global net radiation for July 1979 is similar but algebraically slightly smaller than the new ERBE value for July 1985. In other months, however, the SAB value was the larger. There is, of course, a six-year difference in the Nimbus-7 scanner and the ERBE measurement times. While the SAB net radiation values are about 10 W/m^2 higher than the original Nimbus-7 scanner products, the same qualitative regional variations appear in the global maps. This is illustrated in Section 4 where the two results are first compared and then utilized for a comparison of the cloud and Earth radiation budget monthly averaged fields. For the more detailed regional studies, in Section 5 we have used the available daily values from the old ERB

scanner products. Because our principal interest is in relative comparisons, we have made no attempt to correct the old products.

Two temporal sampling problems occur. While the THIR was on continuously to detect clouds, the ERB instrument was on a three-day-on/one-day-off schedule. Thus, only about 23 days of ERB data are available in a normal month for each TA. Also some of the ERB and/or cloud products are missing from some TA's on various days. To obtain larger measurement samples for statistical evaluation, the targets are grouped in regional blocks of about 20 TA's each. The TA's in a given region are chosen to have roughly similar cloud and net radiation characteristics. After rejecting TA days with some data missing, each region normally has between 300 and 450 TA days available for analysis. A second problem is the fact that in the low and mid-latitudes most target areas are observed only twice a day, once near noon and once near midnight. In a recent comparison of Nimbus ERB wide field of view measurements with contemporary ERBE results, Kyle et al. (1990) found excellent agreement in the mean. The ERBE products were produced using data from two satellites one of which is non-Sun-synchronous and views low and mid-latitude regions at all hours of the day and night over a period of 37 days. Regionally, some errors in the Nimbus ERB diurnal averages are expected to occur because of the limited diurnal sampling. However, the top-of-the-atmosphere solar irradiance is at a maximum at the local noon observing time. Thus, it is particularly important to observe the effect of clouds on the albedo and OLR at this time.

The cloud diurnal averages are affected both by the temporal sampling problem and by the use of both 11.5 μm and 0.37 μm radiances to identify clouds during the day but only the 11.5 μm radiance at night. Even during daylight the 0.37 μm reflectivities are used chiefly to identify low clouds. Low cloud tops

have little thermal contrast with the surface and thus 11.5 μm radiances cannot be used to accurately identify them. The noon to midnight variations in the mid and high level clouds should be represented fairly accurately in the data set but, in the data we use, the noon to midnight low cloud amount changes are suspect.

Due to these problems with the Earth radiation budget and cloud data sets we used, our results should be treated as basically qualitative in nature. The numbers discussed in Section 5 and Tables 1 to 3 will be modestly modified in the future as more accurate data become available. In particular, the albedos will, in most cases, be reduced slightly.

4. THE TROPICAL NET RADIATION BUDGET

Figure 1a and 1b show the Nimbus-7 ERB net radiation map for July 1979 as derived respectively from: (a) the Sorting into Angular Bins (SAB) data set and (b) the original scanner products. Qualitatively, they show the same overall patterns, but the SAB and original global means are, respectively, -4.2 W/m^2 and -13.6 W/m^2. As discussed in Section 3, we expect correct net radiation values to lie between these two results. There are, of course, some regional variations in the differences between the two results. Note the row of local maxima and minima at about 25°N latitude. The positions of the maxima shift slightly from one map to another and relative differences in the peak values vary by over 10 W/m^2. However, the same qualitative pattern of maxima and minima appear on both maps. In discussing the regional differences in the net radiation field we will, in this section, use the SAB results.

The Southern Hemisphere is an energy sink from 10°S latitude to the South Pole. Positive net radiation increases from 10°S latitude to a maximum near 23°N and then slowly declines again towards the North Pole. There is, however, considerable longitudinal structure in the net radiation, and this is particularly so at about 25°N. The major difference is, of course, between the land and ocean as pointed out previously by Randel et al. (1984) and Kyle et al. (1986). Negative net radiation values in the Sahara in July were reported by Raschke and Bandeen (1970). Note the maxima of 130 W/m^2 or larger south of Japan, near the date line, and north of the Dominican Republic. Then note the minimum of -12 W/m^2 in the eastern Sahara. Also note, however, the local minimum of 40 W/m^2 in the Pacific just west of Baja, California. Figure 2 is the Nimbus-7 total noontime cloud cover map for July 1979 derived from the Nimbus-7 cloud data. Over the ocean the net radiation maxima mentioned above occur in regions of about average cloudiness (30% to 60%), but so does the minimum off Baja California.

Figures 3 and 4 show the net radiation and total cloud cover for January 1980. In January, the Northern Hemisphere above 15°N latitude has become a heat sink, while the Southern Hemisphere shows positive net radiation even beyond 60°S latitude. At about 30°S latitude a row of hot spots in the Pacific, south Atlantic, and Indian Oceans occur which are again associated with moderate to average cloud cover.

In the present study we pick six tropical regions to study the varying interrelationships between clouds and net radiation. These regions, identified in Fig. 5, represent the range of interactions that occur in the tropics and subtropics. The general radiation and cloud characteristics of these regions are shown in Table 1. The radiation values shown were derived

from the old Nimbus-7 scanner products during the analysis discussed in Section 5.

Ocean Regions A and B lie just south of the Equator, receive roughly equal amounts of top-of-the-atmosphere insolation, and during these two months (July 1979 and January 1980) have nearly equal net radiation. However, Region A is part of the tropical rain belt around Indonesia and has moderate cloud cover in July and heavy cloud cover in January. On the other hand, Region B lies in the perennial high pressure region west of South America and has below average cloud cover in both July and January.

Region C includes the July high net radiation region in the ocean east of Taiwan, while Region D includes the local minimum off Baja California. In July, they receive about the same solar insolation and during the day the total cloud fraction is the same. However, Region C with relatively thin mid and high level clouds has a net radiation of 117.4 W/m^2, while Region D with brighter, low level stratus clouds has a net radiation of 66.8 W/m^2. Note that noon and midnight OLR for Region D are nearly identical, and the same is true for Region C. Thus, any average noon to midnight shift in the cloud cover is not affecting the OLR.

Regions E and F lie on the land. Region E includes the central Sahara and Arabian deserts, while Region F covers the Congo rain forest and straddles the Equator. Thus, the solar insolation at Region E is considerably larger in July than in January, while the insolation at Region F is only 3% smaller in July than January. However, the cloud cover over the Congo region is about 60% versus about 14% over the central Sahara. Regions E and F represent

tropical extremes in the relationship of clouds and net radiation over land. A more detailed analysis of these three pairs of regions is given below.

5. ANALYSIS OF SELECTED REGIONS

5.1 Procedures

Daily cloud and Earth radiation budget parameters are compared on a target area, $(500\ km)^2$, and regional basis. For each region and month, 12 net radiation bins are set up. The net radiation range from -125 to +125 W/m^2 is divided into ten bins each 25 W/m^2 wide. The two additional bins are net radiation $<-125\ W/m^2$ and net radiation $>125\ W/m^2$. A matrix is formed by considering four total cloud categories for each net radiation bin. These are: percent total target area cloud cover; total cloud cover <20%; ≥20% and ≤80%; and >80%. The characteristics of the clouds in each net radiation bin are then analyzed.

Changes in cloud amounts and/or cloud properties can affect the net radiation. Normally the albedo of clouds is higher than that of the underlying surface. Thus, a decrease in cloud optical thickness and/or in cloud amount tends to decrease the albedo. The higher the cloud altitude the colder the cloud top temperature. Thus, decreasing the cloud top altitude and/or the cloud amount in the tropics tends to increase the OLR. It follows that increasing cloud top altitude and decreasing cloud optical thickness will increase the net radiation in a region. On the other hand, decreasing cloud top altitude and increasing the optical thickness will decrease the net radiation. These points should be kept in mind as the three pairs of study regions are reviewed.

5.2 Southern Tropical Ocean, Regions A and B

These two regions (see Fig. 5) lie just south of the Equator between 0° and 18°S latitude. They receive about the same insolation and absorb approximately the same amount of net radiation (see Table 1), but their climate and cloud cover are very different. As Table 1 indicates, our samples from Region A (Indonesian rain belt) show a 41% average cloud cover in July 1979 when the Sun is north of the Equator, but nearly 90% cloud cover in January 1980. Further, most of the cloud tops were classified as middle or high in both months. In the Nimbus cloud classification, equatorial high cloud tops are over 7 km above sea level, while mid-cloud tops lie between 2 km and 7 km. Region B (eastern Pacific high pressure area) has an average cloud cover of 21% in both months and about half the cloud tops are classified as low. The amount and types of clouds present over the tropical ocean depend not just on the absorbed solar energy, but also on sea-surface temperature and general atmospheric circulation patterns (see, for instance, Emanuel, 1988). The sea-surface temperature is normally lower in Region B than in Region A.

Figure 6 compares for July 1979 the effect of cloud cover on the measured daily top-of-the-atmosphere net radiation for both regions. The total cloud cover is divided into three ranges: relatively clear (0% to 20%), partly cloudy (20% to 80%), and overcast (80% to 100%) target areas. In the relatively clear areas, the existing clouds are almost always low or middle clouds. In the Indonesian region (A), the partly cloudy TA's show a mixture of low, mid, and high cloud tops with the mid-clouds dominating for high net radiation and the high clouds for low net radiation. The overcast areas are chiefly a mixture of high and mid-clouds with the high clouds dominating for

high net radiation (note the increase in cloud fraction at both high and low net radiation). In the western Pacific region there are no overcast regions and almost no high clouds. The cloud tops are slightly higher in the partly cloudy areas compared to relatively clear areas. The high energy (75 to 100 W/m^2) entry in Region B represents a single TA-day with 11% cloud cover during the day followed by 76% cloud fraction (mostly mid and high) at night.

The average albedo and OLR are shown in Fig. 7 for these three cloud cover categories as a function of the net radiation. If all clouds were uniform in albedo and height, then the variations shown in Fig. 7 would reflect changes in cloud fraction. In fact, cloud top temperatures, albedos, and fractions all vary. These plots help illustrate the theme that both cloud type and fraction must be known in order to estimate the effects of the clouds on the net radiation. In Region A, for partly cloudy and overcast areas, both the albedo and OLR decrease as the net radiation increases. This is an optimal situation for high net radiation. More solar energy is absorbed, but less low temperature, longwave radiation is exhausted to outer space. This is done by increasing cloud fraction and cloud top altitude but decreasing cloud albedo. In Region B, the OLR is always relatively high and high net radiation is associated with low albedos. It should be noted that in July the Sun is north of the Equator and that TA's just south of the Equator receive a mean solar insolation of 385 W/m^2 (averaged over 24 hours), while the TA's between 13.5 and 18°S latitude have a mean insolation of only 317 W/m^2. Due to the Sun being lower in the sky, these more southerly TA's also have a slightly higher albedo for identical cloud cover situations. Thus, in July the TA's farther south have a lower average net radiation than do those nearer the Equator. Hence, some of the spread observed in the graphs is due to the range in latitudes included in the study regions. However, the basic interrelationship

between clouds and net radiation shown in these figures is also seen in the individual TA's.

Figure 8 shows a plot of net radiation, albedo, and total noontime cloud cover versus day of the month for target area 903 for July 1979. This is one of the twenty target areas in Region B. On July 2, the first combined observation day, the net radiation has a low value of -56.9 W/m^2 and associated albedo and noontime cloud cover of 34.3% and 56.0%, respectively. A maximum net radiation of +33.4 W/m^2 occurs on July 27 with associated albedo and noontime cloud cover of 12.5% and 12.0%, respectively. Normally albedo and cloud cover variations are in phase with higher values associated with low net radiation and vice versa. The diurnally averaged OLR ranges only from 290 to 303 W/m^2 during the month. However, its variations are not strongly related to changes in net radiation. On the minimum and maximum net radiation days, July 2 and 27, the OLR is, respectively, 291 and 292 W/m^2. An anomaly, with albedo and cloud cover out of phase, occurs on July 11. The net radiation hits a local maximum of 24.2 W/m^2, while the total noon cloud cover increases to 31% with 21% classified as mid-cloud and 10% as low cloud. The diurnal OLR drops some 10 W/m^2, but the albedo changes very little. The presence of the thin, rather low and warm, mid-level cloud appears to have caused the local maximum in the net radiation.

Figure 9 is a similar plot for target area 926 in Region A for January 1980. In this case, the net radiation ranges from -82 to +164 W/m^2, but the total noontime cloud cover is over 90% except on the last two days of the month when it drops to about 50%. High cloud tops dominate except for a few days when mid-clouds are more abundant. Few low clouds can be identified because of the high cloud screen. In general, albedo increases are associated with decreases

in the net radiation and vice versa. This plot indicates that changes in cloud type and thickness can be as important as cloud amount. Three times during the month the net radiation exceeds 160 W/m^2. On the first two days, July 3 and 20, the noon cloud cover is 97% and 88%, respectively, while the albedo is close to 25% and the OLR is about 180 W/m^2. On July 31, however, the noon cloud cover drops to 49% and the albedo to 14%, while the diurnal OLR rises to 224 W/m^2.

Figure 10 shows cloud cover versus net radiation for the two regions in January when the Sun is south of the Equator. Note in Table 1 that both the top-of-the-atmosphere insolation and the net radiation have increased by approximately 100 W/m^2 in both regions. Also, note the different distribution in net radiation measurements between the two locations. In the ocean around southern Indonesia, 41% of the measurements indicate net radiation greater than 125 W/m^2, and the majority of these show overcast conditions. However, a few of the measurements extends beyond -75 W/m^2. The net radiation measurements in Region B, in the eastern Pacific, are grouped fairly tightly about the mean value of 107.9 W/m^2. Only 16.9% of measurements show net radiation greater than 125 W/m^2 and only 5.7% of these belong to the relatively clear category. Thin (relatively dark) cool or cold clouds do appear to increase the net radiation here also.

Sizable diurnal cloud variations occur in some regions. Houze et al. (1981), Johnson and Priegnitz (1981), and Williams and Houze (1987) report that in December 1978 in the ocean off the coast of north Borneo, rain cloud systems would start to form about midnight, peak before noon, and then start to dissipate. Over northern Borneo, however, the cycle reversed and the maximum precipitation occurred near local midnight. Diurnal variations change from

place to place, of course, both over land and ocean (see for instance Kyle et al., 1986).

Perfect daily averages cannot be expected from noon and midnight measurements from either the cloud or Earth radiation budget products. This is particularly true if individual days are considered. On a monthly basis, however, Kyle et al. (1990, Fig. 14) found that for April 1985 the Earth radiation budget products from just the Sun-synchronous NOAA-9 satellite yielded regional diurnal averages within 1% to 5% of those obtained from the combined ERBS and NOAA-9 satellite measurements (Barkstrom et al., 1989). Somewhat cruder diurnal models were used to derive the daily Nimbus-7 Earth radiation products used in this study than were used in the later experiment (see Wielicki and Green, 1989). Thus, errors of several precent may occur in our monthly results while even larger errors may be present in some regions. These diurnal averaging errors in the Nimbus-7 data set are besides the calibration and algorithm errors mentioned in Section 3.

Figures 11a and 11b show the albedo and OLR associated with each of the cloud cover categories as a function of the net radiation. In Region A, the rain region, bright cold (deep convective) tops are associated with low, often negative, net radiation. However, these storm centers are surrounded by large areas of thin middle and high altitude clouds associated with high values of net radiation. This results in a high average net radiation. In Region B, the few clouds present also appear, in the mean, to be relatively neutral. Note from Fig. 10b that a cloud cover minimum of 14% occurs for the 75 to 100 W/m^2 bin and that cloud cover increases for both higher and lower net radiation. However, in Fig. 11b, the albedo decreases monotonically as the net radiation increases.

The types of clouds observed in the two regions at noon during January 1980 are shown in Figs. 12a and 12b as a function of the net radiation. Recall (Section 3) that the cirrus category is a low albedo subset of the high clouds together with the colder mid-altitude clouds, while deep convective is a high albedo subset of just the high clouds. The cirrus and deep convective subsets can be identified only during the day when the TOMS 0.37 μm reflectivities are available (Stowe et al., 1988). In Region A, cloud cover approaches 100% for low net radiation, with high cloud cover alone being over 80%. However, for high net radiation, mid-clouds become as plentiful as high clouds and for net radiation over 125 W/m^2, mid-cloud is the dominant type. The last three net radiation bins (-25 to -100 W/m^2) each contain only one TA-day sample (Fig. 10a). Deep convective clouds are prominent in these bins, but these bins have little impact on the monthly averages. The cirrus clouds cover between 10% and 20% of the area at most values of the net radiation, but there is no marked increase in identified cirrus clouds at high net radiation.

For net radiation greater than 125 W/m^2, the total noon cloud cover is 74.1%, which is broken into high (27.0%), mid (40.9%), and low (6.3%). The deep convective cloud cover is 2.1% and the cirrus is 19.5%. This leaves a cloud cover of 52.5%, most of which either acts to increase the net radiation or is neutral. Apparently, the dominant mid-cloud, which has a low albedo, was considered too warm by the Nimbus cloud algorithm (Stowe et al., 1988) to be classified as "cirrus." Some of it, of course, may be high, very thin cirrus which pass considerable surface radiation and, therefore, are classified as rather warm mid-level cloud. Prabhakara et al. (1988) report that an infrared spectral signal associated with thin cirrus is prominent in this region in December and January.

Figure 12b shows the patterns found in the eastern Pacific high pressure region (B). Here there are few high clouds of any type, while mid and low clouds appear in about equal amounts, except in the few low net radiation regions where mid-altitude clouds dominate. Noontime cloud cover passes through a minimum of 15% for net radiation between 25 and 100 W/m^2 and then increases again up to 25% for net radiation greater than 125 W/m^2. However, the identified cirrus cloud cover is only 0.7% for these warm regions. This suggests that in the tropics thin water clouds may be at least as important as thin cirrus in creating high net radiation regions.

Comparing July and January we see Regions A and B sharply increase their net absorbed energy in January by very different paths. In Region A the cloud cover doubles, high cloud tops increase over 500%, the albedo rises from 22% to 35%, but the OLR drops from 264 W/m^2 to 189 W/m^2. In Region B, the cloud cover remains at about 21%, the albedo actually decreases from 15.3% in July to 14% in January while the OLR also slightly decreases from 292 W/m^2 to 283 W/m^2. The decrease in albedo may be mostly associated with the Sun being higher in the sky in January (see Taylor and Stowe, 1984), while the OLR reduction is probably related to a modest increase in cloud top altitudes.

5.3 Northern Subtropical Ocean, Regions C and D

Here we consider two ocean regions, both with medium cloud cover, but in July, Region C, in the western Pacific, has above average net radiation while Region D, off Baja California, is a net radiation minimum area. Thin mid-altitude stratus are the dominant clouds in Region C while thicker and lower stratus prevail in Region D. In January, the top-of-the-atmosphere insolation

decreases sharply and the two areas no longer stand out on the net radiation map (Fig. 3).

Region C lies between latitudes 18°N and 27°N and stretches from below Japan eastward towards the date line. In July 1979 (see Table 1) it had an average cloud cover of 58% with high and mid-altitude clouds predominant. The relatively low albedo indicates that most of the clouds are fairly thin and perhaps broken in nature. Only in a few cases do bright deep convective cloud appear. This results (Fig. 13a) in a high average net radiation of 117.6 W/m^2, with 80% of the TA-days yielding net radiation in excess of 100 W/m^2. The corresponding values of the albedo and OLR appear in Fig. 14a.

Table 1 indicates that there is very little difference in the noon and midnight OLR although the cloud cover increases from 51% at noon to 64% at midnight. Note, however, that 7% of this increase is classified as low clouds. Now the noon clouds reported in Table 1 were identified using both IR radiances and UV reflectivities, while only the IR radiances were available at midnight. The UV reflectivities were used chiefly to identify warm low clouds. Therefore, Stowe et al. (1989) indicate that while diurnal variations shown in mid and high clouds are fairly trustworthy, those shown in low clouds may be principally due to the presence or absence of the UV reflectivities.

About 42% of the TA-days show a net radiation greater than 125 W/m^2, and for these TA-days the average noontime cloud cover is 40% versus 62% at midnight. At noon, high cloud cover is only 6%, with cirrus also identified as 6%. Again, the majority of clouds in the high net radiation regions are thin (low albedo) but with too warm longwave cloud top radiances to be classified as cirrus.

The associated albedo and OLR for Region C are shown in Fig. 14a. The characteristic decrease in albedo with increasing net radiation appears together with a moderate increase in the OLR. Note in Fig. 13a the monotonic decrease in total cloud cover as the net radiation increases. However, the cloud cover averages 50% or more even for net radiation greater than 125 W/m^2.

Region D lies in the ocean west of Baja, California in about the same latitude range as Region C. In July it receives essentially the same insolation. It also has a moderate cloud cover, but fairly low level clouds dominate. Note the increase from Region C to Region D in both the albedo and the OLR. Thus, the Region D net radiation of 67 W/m^2 is 50 W/m^2 less than that of Region C. Figure 13b shows, for Region D, the distribution of TA-days versus net radiation. It is a relatively flat distribution for positive net radiation but with only one measurement below -50 W/m^2. This is opposed to a rather sharply peaked high energy distribution shown in Region C (Fig. 13a). In Fig. 14b, the OLR shows the small range associated with low cloud regions. Both the cloud cover (Fig. 13b) and the albedo decrease with increasing net radiation.

In July, Regions C and D represent extremes in the effect of tropical oceanic clouds on the net radiation (see Fig. 1). In Region C, the dominant thin mid and high level clouds tend to either aid the net radiation or be neutral, while in Region D the thicker, rather low clouds sharply reduce the net radiation.

In January, these two regions no longer stand out on the net radiation map (Fig. 3). The mean solar insolation has dropped by about 170 W/m^2, and both

regions now are similar heat sinks with a net radiation of about -60 W/m^2. Interestingly, the change in net radiation in Region C is just slightly greater than the change in the top-of-the-atmosphere insolation, while in Region D the change is only about two-thirds of the insolation range. Note in Table 1 that Region C now shows more low cloud tops than does Region D. There has been little change in the total cloud cover in either region, but both cloud type and the solar insolation have changed. The albedo increases in both regions and some of this increase is due to the larger solar zenith angles. However, the increase is noticably larger in Region C indicating an increase in cloud optical thickness. In Region C, the OLR increases by 27 W/m^2 indicating lower effective cloud tops, while in Region D it drops by 27 W/m^2 signalling an increase in the effective cloud top altitude.

These two regions, with roughly equal cloud cover, illustrate the varying effect of different cloud types on the net radiation. In winter both are heat sinks, with somewhat different cloud types that yield the same net radiation. In the summer high, thin clouds make Region C an efficient heat absorber, but the low, relatively thick clouds in Region D make it a poor heat absorber.

5.4 Land: Desert and Tropical Rain, Regions E and F

Land regions tend to be more variable than ocean regions, and the Sahara and Arabian deserts appear in extreme contrast to the African portion of the equatorial rain belt. Water has a high heat capacity and ocean regions have the potential to store large amounts of heat, move excess heat by convection, and dissipate it by evaporation. Evaporation puts water vapor into the air, changing the air's physical properties including its ability to absorb and transmit radiation. In addition, the probability for cloud formation is

enhanced. Rain forests contain large amounts of water and, thus, to a large degree share these characteristics with ocean regions. Deserts, however, are normally dry with low heat capacity and heat storage capabilities. Thus, they react quickly to the presence or absence of solar radiation. They use wind and radiative cooling as the major means of disposing of excess heat. Because of the lack of moisture it is relatively difficult over the desert to create local cloud fields.

Lying at different latitudes, the insolation in Region E (central Sahara) decreases by 35% from July to January, while that in Region F (rain belt) increases by 4% (see Table 1). Therefore, it is not surprising that their seasonal changes are not in phase. It should be noted that Region E is at the same latitude as the ocean Regions C and D, and its seasonal variations should most properly be compared to theirs.

Table 1 indicates that the central Sahara has a mean cloud cover of 9.3% in July which increases to 18.5% in January, with the mid and high altitude noon cloud cover changing from 2% in July to 11.3% in January. While the solar insolation decreases by 160.4 W/m^2 from July to January, the net radiation drops only about half as much. Comparing with colatitude regions C and D in July, we see that the bright, hot desert is a very weak (8.3 W/m^2) energy absorber compared to 117.8 W/m^2 for Region C and 66.8 W/m^2 for Region D. In January, though, all three are comparable energy sinks (-60 to -72 W/m^2).

The African rain region (F) has a total cloud cover of approximately 60% in both July and January, but the net radiation still changes with the season. The solar insolation increases by 16.5 W/m^2 from July to January, but the net radiation jumps 43 W/m^2 or 2.5 times as much. The increase in net radiation

is associated with changes in the cloud fields. The average noon/midnight cloud amount is approximately 60% in both months, but in January both the albedo and the OLR have decreased compared to July. This is related to a phase change in the diurnal cloud cycle. In January, the noontime cloud fraction has decreased and the midnight cloud fraction has increased compared to July.

Figure 15 shows the population (TA-days) versus net radiation for Regions E and F in July 1979. In the desert region (E), the relatively clear regions dominate. Dry desert has a relatively high albedo which, however, varies considerably with location. Note in July (Fig. 15a) that cloud cover decreases when the net radiation decreases. This is the opposite of what is observed in ocean or rain forest regions. Figure 16a shows the associated albedo and OLR. For the mostly clear regions, both the OLR and albedo increase with decreasing net radiation.

In the rain region (Figs. 15b and 16b) the clouds dominate. The mostly clear regions are grouped tightly about the mean net radiation of 13.9 W/m^2, but both the high and low net radiation measurements are associated chiefly with the partly cloudy and overcast conditions. The cloud cover shows a U-shape with the minimum at the mean net radiation and then increases in both the high and low net radiation directions. Both the albedo and OLR (Fig. 16b) tend to decrease with increasing net radiation.

The graphs for January are similar in form to those for July but with a shift to lower net radiation over the Sahara and to higher values over the African rain belt. Figures 17 and 18, for the rain belt only, illustrate this shift. There are still a few negative net radiation measurements shown in Fig. 17,

but they represent less than 4% of the observations. In Fig. 18, in the (-25 to -50 W/m^2) bin, the albedo is greater for the diurnal partly cloudy case (20 to 80% cloud cover) than for the overcast case (cloud cover >80%). There is only one target area day in each category. The overcast TA was 100% cloud covered both at noon and midnight, but 22% of the daytime clouds were classified as cirrus (low albedo). The partly cloudy case was 84% cloud covered at noon, but the cloud cover decreased to 47% at midnight. In the partly cloudy case, the daytime clouds were all associated with high albedos. This case emphasizes that albedo and total cloud fraction are not always closely related.

The phase of the diurnal cloud cycle can effect the net radiation. A relatively clear day followed by overcast conditions at night causes the net radiation to increase. The reverse phase will decrease the net radiation. A clear day allows the absorption of a large percentage of the top-of-the-atmosphere insolation. A high percentage of mid or high clouds at night will sharply reduce the loss of radiative energy at night. Figure 19 shows for the six study regions the difference (noon OLR minus midnight OLR) as a function of the net radiation for July 1979. Figure 20 shows the same quantity for January 1980. Consistently the four ocean regions and the African rain area indicate that for algebraically small net radiation the noontime OLR is smaller than the midnight OLR. This indicates a decrease in cloud amount and/or altitude at night. For high net radiation, however, the reverse occurs; the midnight radiation is lower than the noon OLR. This high net radiation effect is visible also in the desert. The albedo plots (Figs. 7, 11, 14, 16, and 18) also indicate that the low net radiation areas are brighter at noon than the high net radiation areas. Excepting desert regions, this higher albedo is due to a combination of more and thicker clouds.

Figures 8 and 9 indicate temporal patterns of cloud fields moving across the study target areas causing the net radiation to vary as cloud types and cloud cover change. It has also been indicated that the albedo of the region is one of the most important factors governing the net radiation. Thus when we sort by net radiation, bright scenes will be more numerous at low net radiation. Similarly, low OLR at night will tend to be associated with higher net radiation provided the albedo does not dominate. However, it is the populations (see Figs. 6, 10, 13, 15, and 17) which govern the importance of the high or low nighttime OLR.

In the African rain area (F), the phase of the diurnal cloud cycle is obviously an important factor. The average noon OLR is 12.5 W/m^2 larger than the midnight OLR in July, and this increases to 21.2 W/m^2 in January. Further, in both months over 80% of the observed cases had lower OLR at midnight. This actually is a common characteristic of both cloudy and clear land regions and is driven by the radiative cooling of the surface. However, here the increased cloud cover associated with the decrease in OLR indicates that diurnal cloud cover/type changes help force the diurnal OLR cycle. In the four ocean regions there is little difference in the average noon and midnight OLR (Table 1) in both July 1979 and January 1980. However, if examined in detail all four regions (A, B, C, and D) in January and Region C, east of Taiwan, in July have numerous high net radiation measurements where diurnal changes in the cloud cover/type decrease the OLR at midnight by 6 to 20 W/m^2 compared to noon. Thin, mid-altitude clouds are the dominant clouds identified over target areas with high net radiation.

In the desert region (E) the low heat capacity of the dry, sandy surface is the dominant factor in the diurnal changes in the OLR. The surface temperature rises steadily during the day and then drops rapidly after sundown. However, as shown in Table 1, there is a significant increase in cloud cover at night, and this undoubtedly contributes to the noon minus midnight difference in the OLR.

The incident solar insolation is a maximum at local noon. Thus, while the Nimbus-7 noon and midnight measurements cannot entirely define the diurnal cycle, they can indicate its effect on the net radiation. A fully quantitative analysis of the effect of the diurnal cloud cycle on the net radiation will require data sets with more adequate diurnal sampling.

6. Comparison with Some Other Equatorial Regions

To set the equatorial study regions in context, we briefly review some neighboring regions. This is not, however, a survey of the entire tropics. The first group of seven regions we consider lie in the ocean between 0° and 18°S latitude and stretch westward from the coast of Peru past Australia; they include study Regions A and B. The second group of three regions consist of the tropical rain belt in South America, Africa (study Region F) and the island continent of Indonesia. These comparison regions are indicated on the map in Fig. 5. Using these additional study regions plus the global maps (Figs. 1 through 4) it is shown that aside from central Sahara (Region E) the regions studied in Section 5 are not atypical.

Table 2 lists the characteristics of the seven southern equatorial ocean regions in July and January. The average top-of-the-atmosphere insolation

varies from about 352 W/m^2 in July to 455 W/m^2 in January. In July the net radiation has a deep minimum of -54.3 W/m^2 in Region 1 just off the Peruvian coast. There is a corresponding ocean maximum of 38.4% in the albedo, and the diurnal cloud cover averages 64.4%. Fairly warm, mid-altitude clouds dominate and there are almost no high clouds. Thus, the clouds sharply increase the reflected solar radiation without greatly decreasing the OLR. Region 2 has an intermediate net radiation of -10.3 W/m^2. The other 5 regions have positive net radiation ranging from 3 to 10 W/m^2 despite the fact that the total cloud cover ranges from 21% to 70%. In January, with increased solar insolation, all seven regions have high net radiation with a range of only 13 W/m^2 among them. The range in total cloud cover increases in January and varies from 20% to 90%. Thus, study Regions A (7) and B (3) illustrate that in the tropics, wide ranges in cloud types and cover may result in the same net radiation.

The characteristics of the three equatorial land rain regions are given in Table 3. Although all three straddle the Equator, the latitude distribution of the regions vary depending on local land configurations and climate. This results in a slightly wider range in solar insolation among these three regions than occurred among the previous seven regions. This is particularly so in January where the range amounts to 20 W/m^2. The centroid of the South and Central American region (10) lies farther north than that of the other regions, so that its solar insolation is actually 5 W/m^2 higher in July than in January. Similarly its net radiation is a little larger in July. As might be expected, the Indonesian rain area has a slightly higher net radiation than the other two. Its climate is dominated by the warm surrounding seas. For the equatorial regions, the Sun is most directly overhead at the spring and fall equinoxes so that July and January do not represent extremes in the solar insolation as they do at higher latitudes. However, even with the limited

range in solar insolation shown, variations in the net radiation consistently track changes in the top-of-the-atmosphere insolation.

The sharp decrease in net radiation caused by bright low or medium altitude clouds with reasonably warm cloud tops is shown both by study Region D in July and Region 1 (Table 2) in January. Such regions are not common in the tropics, but they do occur. As shown in Figs. 1 and 3, extreme highs in the net radiation, such as in study Region C east of Taiwan, tend to occur a little poleward of the subsolar point. A seasonal survey will be required to see if such hot spots occur often over equatorial oceans.

The central Sahara/Arabian deserts, Study Region E, does appear to be unique because of its immense continental area with very high surface albedos. These produce a large net radiation sink in the northern tropics with important climatological ramifications (see for example Smith, 1986). However, the net radiation in this region is dominated not by clouds but by its surface characteristics.

7. Conclusions and Discussion

A comparison of the Nimbus-7 cloud and Earth radiation budget data sets in the tropics during the months of July 1979 and January 1980 illustrate the wide effects that clouds have on the tropical radiation budget. A brief general survey of the tropics was followed by a detailed examination of six study regions, each three to six million square kilometers in area (Fig. 5). Daily values of the cloud and radiation budget parameters were examined. These regions exemplify the range in cloud/net radiation interactions in the tropics. Our conclusions are:

1. Despite cloud cover ranging up to 90%, tropical rain and monsoon areas are regions of high net positive radiation. The bright, deep convective storm centers tend to have negative net radiation, but these are surrounded by and temporally alternate with large bands of thin medium and high altitude clouds associated with very high net positive radiation. This combination results in high positive values for the regional net radiation.

2. Both in the tropical rain regions and over the tropical ocean in general, radiation budgets are dominated not by cloud amount but by cloud types.

   - With the same solar insolation, ocean regions with average cloud cover ranging from 20% up to 90% can and often do show the same monthly averaged net radiation.

   - Large regions of bright (thick) low or low-medium altitude clouds over the ocean sharply depress the net radiation by sharply increasing the reflected solar radiation without markedly reducing the OLR. In the tropics and subtropics, such regions occur off the west coast of Africa and the Americas and are associated with relatively low sea-surface temperatures.

   - In July and January the highest net radiation regions tend to lie just poleward of the subsolar point. They have about

50% cloud cover. The associated clouds have low cloud top temperatures and moderate to low albedos.

3. Over the tropical ocean, the highest net radiation days usually show a marked increase of clouds with a low albedo and cool or cold cloud top temperatures. The effective cloud top temperatures derived from the Nimbus-7 THIR 11.5 μm radiances indicate that they usually lie between 2 and 4.5 km above sea level. This would tend to indicate mid-altitude stratus clouds. However, many of these clouds may actually be thin and perhaps broken high altitude cirrus which allow some warm surface radiation to pass through.

4. The African rain region in July and January shows a marked increase in high cloud cover at midnight compared to noon. This is associated with a considerable drop in the OLR, which in turn increases the diurnal net radiation. Although the Nimbus noon/midnight measurements can identify diurnal cloud changes and some of their affect on the radiation budget, better diurnal information is needed.

5. As expected, the net radiation in the central Sahara is little affected by clouds. Unlike the other study regions, the lowest net radiation is associated with the lowest cloud cover. Interestingly Ramanathan et al. (1989) listed the Sahara in April as one region where the clouds tend to increase the net radiation. Our findings do not contradict this.

6. In the subtropics and at higher latitudes where there are large seasonal variations in the insolation, regional variations in the net radiation are large for high insolation and moderate for low insolation values.

From a climatological point of view our study indicates that tropical clouds can have strong effects, both positive and negative, on the average net radiation. At present, there is a tendency for the positive and negative effects to balance for the tropics as a whole (see also Ramanathan et al., 1989 and Ardanuy et al., 1989a). The ENSO event of 1982/83 caused large perturbations in the normal tropical albedo and OLR fields, but relatively small changes in the net radiation field (Ardanuy et al., 1987; Ardanuy and Kyle, 1986). Tropical climate changes which increase the desert areas and/or thick low stratus over the ocean would, presumably, act to decrease the absorbed net radiation. The effect on the net radiation of a general increase in tropical cloudiness would depend strongly on the cloud types involved.

In the future we plan to complete our survey of both tropical and extratropical regions and also to include the months of April and October in order to review the changes in all four seasons. In addition, we hope to check our conclusions both with an improved Nimbus-7 scanner Earth radiation budget data set, scheduled to become available in the fall of 1989 (Hucek et al., 1989), and with the new Earth Radiation Budget Experiment (ERBE) data set (Barkstrom et al., 1989).

ACKNOWLEDGMENTS

The work on this research by one of us (H.L.D.) was supported by grant NAG5-1012 from the National Aeronautics and Space Administration. The Nimbus-7 cloud data set was prepared by the Nimbus-7 Cloud Data Processing Team and the Earth Radiation Budget (ERB) data set by the ERB Nimbus-7 Experiment Team and the ERB Data Processing Team. We particularly acknowledge the work of Larry Stowe on both data sets and of Herbert Jacobowitz on the ERB data set. Both are with the National Environmental Satellite, Data, and Information Service of the National Oceanic and Atmospheric Administration. We thank the anonymous reviewers for pointing out portions of the original manuscript that needed clarification. We also thank Philip Ardanuy for reading and commenting on the manuscript and Brenda Vallette for preparing the typescript; both are with Research and Data Systems Corporation.

REFERENCES

Ardanuy, P. E. and H. L. Kyle, 1986: El Niño and outgoing longwave radiation: observations from Nimbus-7 ERB, Mon. Wea. Rev., 114, 415-433.

Ardanuy, P. E., H. L. Kyle, R. R. Hucek, and B. S. Groveman, 1987: Nimbus-7 Earth radiation budget wide field of view climate data set improvement, 2. Deconvolution of the Earth radiation budget products and consideration of the 1982-83 El Niño event, J. Geophys. Res., 92, 4125-4143.

Ardanuy, P. E., L. L. Stowe, A. Gruber, and M. Weiss, 1989a: Shortwave, longwave, and net cloud-radiative forcing as determined from Nimbus-7 observations, IRS '88: Current Problems in Atmospheric Radiation, Proceedings of the International Radiation Symposium, Lille France, August 18-24, 1988 (A. Deepak Publishing, Hampton, Virginia), 232-235.

Ardanuy, P. E., L. L. Stowe, A. Gruber, M. Weiss, and C. S. Long, 1989b: Longwave cloud radiative forcing as determined from Nimbus-7 observations, J. Climate, 2, 766-799.

Arking, A. and S. K. Vemury, 1984: The Nimbus-7 ERB data set: a critical analysis, J. Geophys. Res., 89, 5089-5097.

Barkstrom, B., E. Harrison, G. Smith, R. Green, J. Kibler, R. Cess, and the ERBE Science Team, 1989: Earth Radiation Budget Experiment (ERBE), archival and April 1985 results, Bull. Am. Meteor. Soc., 70, 1254-1262.

Cess, R. D. and G. L. Potter, 1987: Exploratory studies of cloud radiative forcing with a general circulation model, Tellus, 39A, 460-473.

Emanuel, K. A., 1988: Toward a general theory of hurricanes, American Scientist, 76, 370-379.

Groveman, B. S., H. L. Kyle, and D. T. Bolvin, 1988: Earth radiation budget products from the Nimbus-7 ERB scanning radiometer obtained using a sorting into angular bin algorithm, EOS, 315.

Hartmann, D. L. and D. A. Short, 1980: On the use of Earth radiation budget statistics for studies of clouds and climate, J. Atmos. Sci., 37, 1233-1250.

Henderson-Sellers, A., G. Seze, F. Drake, and M. Desbois, 1987: Surface-observed and satellite-retrieved cloudiness compared for the 1983 ISCCP special study area for Europe, J. Geophys. Res., 92, 4019-4034.

Houze, R. A., Jr., S. G. Geotis, F. K. Marks, Jr., and A. K. West, 1981: Winter monsoon convection in the vicinity of north Borneo, Part I: Structure and time variation of the clouds and precipitation, Mon. Wea. Rev., 109, 1595-1614.

Hucek, R. R., H. L. Kyle, and R. A. Frey, 1989: Nimbus-7 Earth radiation budget products using maximum likelihood cloud estimates, EOS, 70, 295-296.

Hwang, P. H., L. L. Stowe, H. Y. M. Yeh, H. L. Kyle, and the Nimbus-7 Cloud Data Processing Team, 1988: The Nimbus-7 global cloud climatology, Bull. Am. Meteor. Soc., 69, 743-752.

Jacobowitz, H., H. V. Soule, H. L. Kyle, F. B. House, and the Nimbus-7 ERB Experiment Team, 1984: The Earth Radiation Budget (ERB) Experiment: An overview, J. of Geophys. Res., 89, 5021-5038.

Johnson, R. H. and D. L. Priegnitz, 1981: Winter monsoon convection in the vicinity of north Borneo, Part II: effects on large-scale fields, Mon. Wea. Rev., 109, 1615-1628.

Kyle, H. L., Ardanuy, P. E., and E. J. Hurley, 1985: The status of the Nimbus-7 ERB Earth radiation budget data set, Bull. Amer. Meteor. Soc., 66, 1378-1388.

Kyle, H. L., A. Mecherikunnel, P. E. Ardanuy, L. Penn, B. Groveman, G. G. Campbell, and T. H. Vonder Haar, 1990: A comparison of two major Earth radiation budget data sets, J. Geophys. Res., (in press).

Kyle, H. L., K. L. Vasanth, and the Nimbus-7 ERB Experiment Team, 1986: Some characteristics differences in the Earth's radiation budget over land and ocean derived from the Nimbus-7 ERB experiment, J. Climate Appl. Meteor., 25, 958-981.

Platt, C. M. R., 1981: The effect of cirrus of varying optical depth on the extraterrestrial net radiative flux, Quart. J. R. Met. Soc., 107, 671-678.

Prabhakara, C., R. S. Fraser, G. Dalu, M. C. Wu, and R. J. Curran, 1988: Thin cirrus clouds: seasonal distribution over oceans deduced from Nimbus-4 IRIS, J. Appl. Meteor., 27, 374-399.

Ramanathan, V., R. D. Cess, E. F. Harrison, P. Minnis, B. R. Barkstrom, E. Ahmad, and D. Hartman, 1989: Cloud-radiative forcing and climate insights from the Earth radiation budget experiment, Science, 243, 57-63.

Randel, D., L. Smith, T. Vonder Haar, and G. Campbell, 1984: Analysis of Nimbus Earth radiation budget measurements for climate study, Proceedings of the International Radiation Symposium, Perugia, Italy, 21-28 August 1984 (A. Deepak Publishing, Hampton, Virginia), 206-209.

Raschke, E., and W. R. Bandeen, 1970: The radiation balance of the planet Earth from radiation measurements of the satellite Nimbus II, J. Appl. Meteor., 9, 215-238.

Schiffer, R. A. and W. B. Rossow, 1983: The international satellite cloud climatology project: the first project of the world climate research program, Bull. Amer. Meteor. Soc., 64, 779-784.

Slingo, J. M., 1987: The development and verification of a cloud prediction scheme for the ECMWF model, Quart. J. R. Met. Soc., 113, 899-927.

Smith, E. A., 1986: The structure of the Arabian heat low, Part II: bulk tropospheric heat budget and implications, Mon. Wea. Rev., 114, 1084-1102.

Stowe, L. L., C. G. Wellemeyer, T. F. Eck, H. Y. M. Yeh, and the Nimbus-7 Cloud Data Processing Team, 1988: Nimbus-7 global cloud climatology, Part I: Algorithms and validation, J. Climate, 1, 445-470.

Stowe, L. L., H. Y. M. Yeh, T. F. Eck, C. G. Wellemeyer, H. L. Kyle, and the Nimbus-7 Cloud Data Processing Team, 1989: Nimbus-7 global cloud climatology, Part II: First year results, J. Climate, 2, 671-709.

Susskind, J., D. Reuter, and M. T. Chahine, 1987: Cloud fields retrieved from analysis of HIRS2/MSU sounding data, J. of Geophys. Res., 92, 4035-4050.

Taylor, V. R. and L. L. Stowe, 1984: Reflectance characteristics of uniform Earth and cloud surface derived from Nimbus-7 ERB, J. Geophys. Res., 89, 4987-4996.

Wielicki, B. A. and R. N. Green, 1989: Cloud identification for ERBE radiative flux retrieval, J. Appl. Meteor., 28, 1131-1146.

Williams, M. and R. A. Houze, 1987: Satellite-observed characteristics of winter monsoon cloud clusters, Mon. Wea. Rev., 115, 505-519.

WMO, 1969: International Cloud Atlas, reprint of 1956 edition, (World Meteorological Organization, Geneva), 137 pp.

Table 1

Radiation and Cloud Characteristics of Six Tropical Study Regions in July 1979 and January 1980

REGION	NR W/m^2	A %	OLR F_{AV} W/m^2	F_D W/m^2	F_N W/m^2	CLOUDS T_C %	$T_C(D)$ %	$T_C(N)$ %	$L_C(D)$ %	$M_C(D)$ %	$H_C(D)$ %	$L_C(N)$ %	$M_C(N)$ %	$H_C(N)$ %	I_S W/m^2
JULY 1979															
A	10.1	22.4	263.8	264.0	263.5	41.0	37.9	44.1	11.1	19.1	7.7	13.8	23.0	1.3	352.87
B	7.0	15.0	291.9	292.1	291.8	21.3	20.8	21.8	9.4	11.3	0.1	8.2	13.4	0.2	351.7
C	117.6	22.2	240.3	240.7	239.9	57.8	51.2	64.3	10.0	25.0	16.1	17.8	29.4	17.1	460.29
D	66.8	26.7	272.5	272.9	272.0	42.5	51.7	33.2	30.1	20.2	1.5	3.6	27.9	1.7	462.94
E	8.3	31.9	304.8	322.9	282.6	9.3	5.9	12.6	3.8	1.8	0.2	2.0	9.4	1.2	459.94
F	13.9	36.1	240.3	246.6	234.1	60.4	59.5	61.3	7.6	38.8	13.1	4.7	35.3	21.3	398.1
JANUARY 1980															
A	106.1	35.2	188.7	189.2	188.2	89.5	84.8	94.3	4.3	35.4	45.0	8.8	36.9	48.6	454.56
B	107.9	14.0	283.3	285.3	281.1	20.5	20.7	20.4	10.1	9.4	1.1	7.7	11.7	1.0	454.88
C	-62.6	31.2	267.6	269.6	266.0	51.7	48.1	55.4	16.3	28.1	3.6	18.0	32.2	5.2	298.14
D	-60.1	34.6	245.8	246.8	245.0	51.0	51.3	50.7	8.4	30.4	12.5	3.0	34.6	13.3	284.04
E	-72.2	37.2	259.7	275.5	246.8	18.5	14.5	22.5	3.2	7.2	4.1	0.2	18.5	3.8	299.53
F	56.5	31.3	228.3	238.9	217.7	59.3	51.1	67.5	2.4	32.7	15.9	3.3	36.5	27.7	414.6

In the tropics, the Nimbus cloud altitude classification is: cloud tops below 2 km-low, cloud tops between 2 km and 7 km-mid, and cloud tops above 7 km-high. NR = net radiation, A = albedo, D = day, N = night, T = total, and L, M, H = low, mid, high. I_S = solar insolation.

Table 2
Radiation and Cloud Characteristics of Seven South Tropical Ocean Regions: Latitude Range 0° to 18°S

Region	No. of Target Areas	TA-Days	Longitude Range	I_S (W/m^2)	NR (W/m^2)	A (%)	OLR (W/m^2)	T_C (%)	$L_C(D)$ (%)	$M_C(D)$ (%)	$H_C(D)$ (%)
July											
1	10	222	76.5° to 90°W most land excluded	347.2	-54.3	38.2	269.0	64.4	19.6	48.0	0.4
2	20	422	90° - 112.5°W	351.7	-10.3	22.3	283.4	40.8	10.7	27.8	0.2
3=B	20	438	112.5° - 135°W	351.7	7.0	15.0	291.9	21.3	9.4	11.3	0.1
4	20	392	135° - 157.5°W	351.7	4.9	16.3	289.4	23.4	11.3	9.8	1.1
5	20	360	157.5° - 180°W	351.7	3.2	20.6	276.1	36.0	13.1	14.2	4.5
6	20	251	180° - 157.5°E	351.7	9.8	30.8	233.7	70.0	13.3	28.4	21.8
7=A	24	419	157.5° - 112.5°E most land excluded	352.9	10.1	22.4	263.8	41.0	11.1	19.1	7.7
January											
1	10	158	76.5° to 90°W most land excluded	457.9	98.9	19.2	271.0	46.5	9.5	28.7	1.6
2	20	338	90° - 112.5°W	454.9	97.9	16.5	282.0	35.0	7.2	24.3	0.2
3=B	20	350	112.5° - 135°W	454.9	107.9	14.0	283.3	20.5	10.1	9.4	1.1
4	20	319	135° - 157.5°W	454.9	101.9	22.2	251.9	43.4	9.4	16.8	13.9
5	20	259	157.5° - 180°W	454.9	106.9	25.0	234.5	63.2	10.5	24.3	22.7
6	20	268	180° - 157.5°E	454.9	110.7	27.5	218.9	76.0	9.9	32.9	27.1
7=A	24	404	157.5° - 112.5°E most land excluded	454.6	106.1	35.2	188.7	89.5	4.3	35.4	45.0

NR = net radiation; A = albedo; D = day; N = night; t = total; L, M, H = low, mid, high; and I_S = solar insolation.

Table 3
Radiation and Cloud Characteristics of Three Tropical Land Rain Regions

Region	Parameter	No. of Target Areas	TA-Days	Latitude Range	Longitude Range	I_S (W/m^2)	NR (W/m^2)	A (%)	OLR (W/m^2)	T_C (%)	$L_C(D)$ (%)	$M_C(D)$ (%)	$H_C(D)$ (%)
					July								
8=(F)	Africa/Rain	22	435	9°S - 9°N	Variable 13.5°W - 31.5°E	398.1	13.9	36.1	240.3	60.4	7.6	38.8	13.1
9	Indonesia/ Malaysia	19	373	9°S - 13.5°N	Variable 94.5°E - 148.5°E	392.1	37.8	34.7	218.1	75.0	8.6	37.4	26.1
10	SA-Amazon/ Central Am.	30	607	9°S - 18°N	Variable 45°W - 99°W	405.0	30.8	34.2	235.5	63.7	7.4	40.7	15.4
					January								
8=(F)	Africa/Rain	22	318	9°S - 9°N	Variable 13.5°W - 31.5°E	414.6	56.5	31.3	228.3	59.3	2.4	32.7	15.9
9	Indonesia/ Malaysia	19	332	9°S - 13.5°N	Variable 94.5°E - 148.5°E	420.5	68.7	37.7	193.2	83.7	2.9	38.2	39.3
10	SA-Amazon/ Central Am.	30	534	9°S - 18°N	Variable 45°W - 99°W	400.2	23.0	35.4	235.6	62.9	8.0	41.3	14.5

NR = net radiation; A = albedo; D = day; N = night; t = total; L, M, H = low, mid, high; and I_S = solar insolation.

FIGURE CAPTIONS

Figure 1. Monthly averaged net radiation for the month of July 1979 derived from (a) the Nimbus-7 Earth Radiation Budget scanner observations by the Sorting into Angular Bins (SAB) algorithm and (b) the original scanner algorithm.

Figure 2. Monthly averaged noon cloud cover for July 1979 as recorded in the Nimbus-7 cloud data set.

Figure 3. Nimbus-7 observed monthly averaged net radiation for January 1980 (see Figure 1).

Figure 4. Monthly averaged noon cloud cover for January 1980 (see Figure 2).

Figure 5. Map showing the six study regions A to F defined in Table 1, as well as the comparison regions 1 to 10 discussed in Section 6 and Tables 2 and 3. There is an overlap between the two groups: 3=B, 7=A, and 8=F. Region A extends beyond both the northeast and northwest coasts of Australia. Region 9 covers land regions in New Guinea, Indonesia, and the Malay Peninsula; it is in several separate pieces and includes some nearby ocean. The individual target areas in each region are also shown.

Figure 6. Bar chart showing the percent of TA days with the indicated net radiation for July 1979 for (a) study Region A, ocean north of Australia, and (b) study Region B, ocean west of Peru (see Fig. 5). Between -125 and +125 W/m^2 the net radiation is divided into

10 bins each 25 W/m^2 wide. Two additional bins show net radiation > +125 or < -125 W/m^2. Three target area cloud cover categories are also indicated: cloud cover <20%, ≥20% but ≤80%, and ≥80%. The total TA-day population (Pop) and mean target area cloud cover (T-CLD) for each bin is given in tabular form above the bar chart. The top table lists the general characteristics of the region: mean net radiation (NR), diurnally averaged outgoing longwave radiation (OLR), albedo (A), and cloud cover (cloud). The total number of target area (TA) days used in the study are also given.

Figure 7. Diurnally averaged albedo and outgoing longwave radiation (OLR) versus net radiation for three categories of target area cloud cover: cloud cover <20%; ≥20% but ≤80%; >80%. Plots are for July 1979 for (a) study Area A and (b) study Area B. The populations corresponding to each cloud category are shown in Fig. 6.

Figure 8. Plot of noon cloud cover and diurnally averaged albedo and net radiation versus day of the month for July 1979 for Nimbus-7 ERB target area No. 903 in study Region B, ocean west of Peru (see Fig. 5). The center of the target area lies at latitude 6.75°S, longitude 123.75°W.

Figure 9. Plot of noon cloud cover and diurnally averaged albedo and net radiation versus day of the month for January 1980 for target area 926, latitude 6.75°S, longitude 128.25°E, in study Region A north of Australia (see Fig. 5).

Figure 10. Bar chart of the percent of TA days with the indicated net radiation distribution during January 1980 for (a) study Region A and (b) study Region B. Refer to Fig. 6.

Figure 11. Albedo and outgoing longwave radiation (OLR) versus net radiation for three cloud cover categories for January 1980, (a) study Region A and (b) study Region B. Refer to Fig. 7.

Figure 12. Noon cloud types versus diurnal net radiation for January 1980 (a) study Region A, ocean north of Australia and (b) study Region B, ocean west of Peru.

Figure 13. Bar chart of the percent of TA days with the indicated net radiation during July 1979 for (a) study Region C, ocean east of Taiwan and (b) study Region D, ocean west of Baja California. Refer to Fig. 6.

Figure 14. Plots of albedo and outgoing longwave radiation (OLR) versus net radiation for three cloud cover categories for July 1979 for (a) study Region C and (b) study Region D. Refer to Fig. 7. The location of the study regions are given in Fig. 5.

Figure 15. Bar chart showing the percent of TA days with the indicated net radiation for July 1979 for (a) study Region E, central Sahara/Arabian Desert and (b) study Region F, African rain belt. Refer to Fig. 6.

Figure 16. Plot of albedo and OLR versus net radiation for three cloud cover categories during July 1979 for (a) study Region E, desert and (b) study Region F, African rain belt. Refer to Fig. 7.

Figure 17. Percent of TA-days with the indicated net radiation for January 1980 for the African rain belt (F). Refer to Fig. 6.

Figure 18. Plot of albedo and OLR versus net radiation for three cloud cover categories during January 1980 for (a) study Region E, desert, and (b) study Region F, African rain belt. Refer to Fig. 7.

Figure 19. Plot of noon minus midnight outgoing longwave radiation (OLR) versus net radiation for the six study areas A to F (Fig. 5) during July 1979.

Figure 20. Similar to Figure 19, but for January 1980.

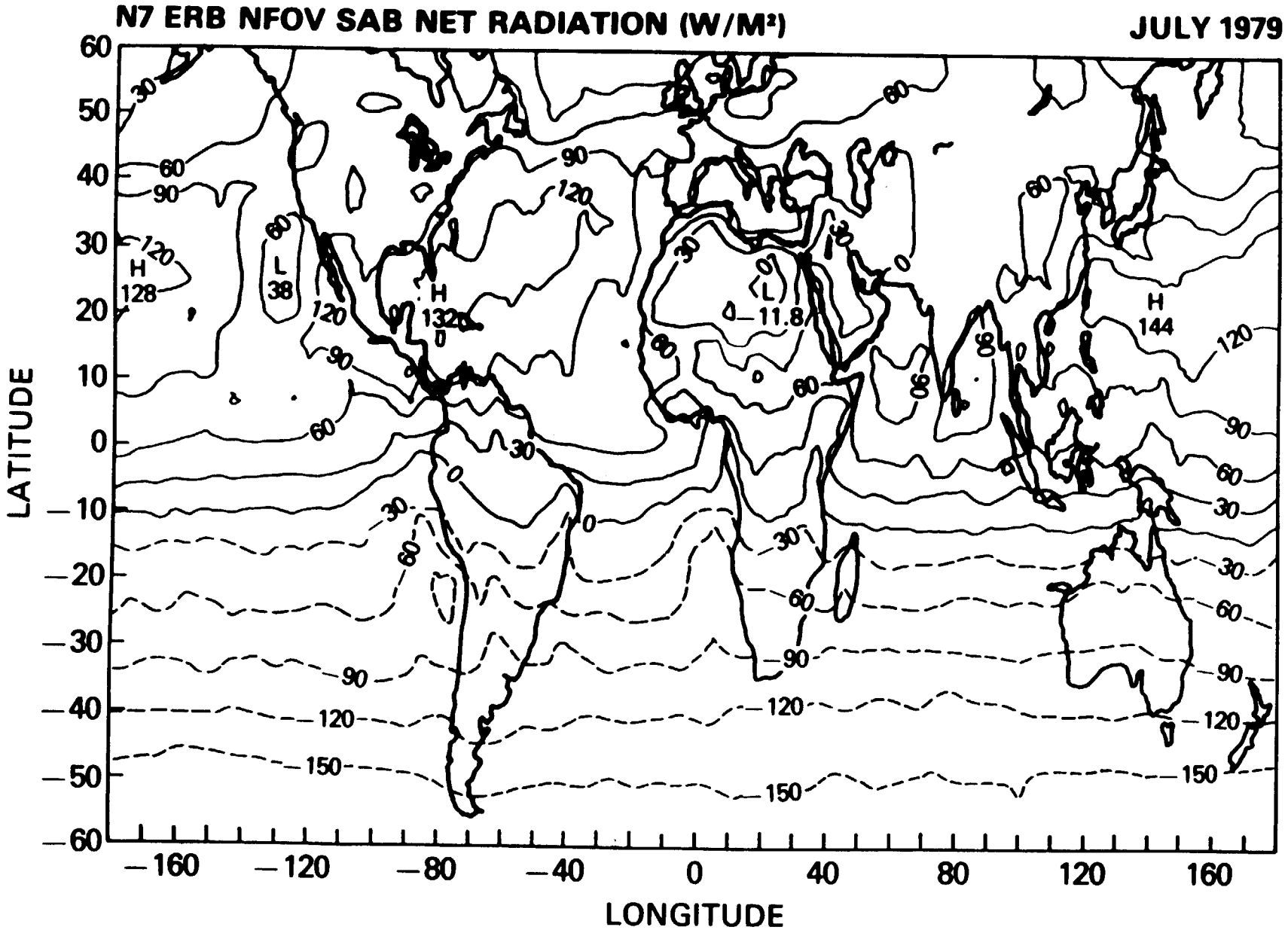
N7 ERB NFOV SAB NET RADIATION (W/M²)
JULY 1979
LATITUDE
LONGITUDE
60
50
40
30
20
10
0
−10
−20
−30
−40
−50
−60
−160
−120
−80
−40
0
40
80
120
160
H
128
L
38
H
132
L
−11.8
H
144

Fig. 1a

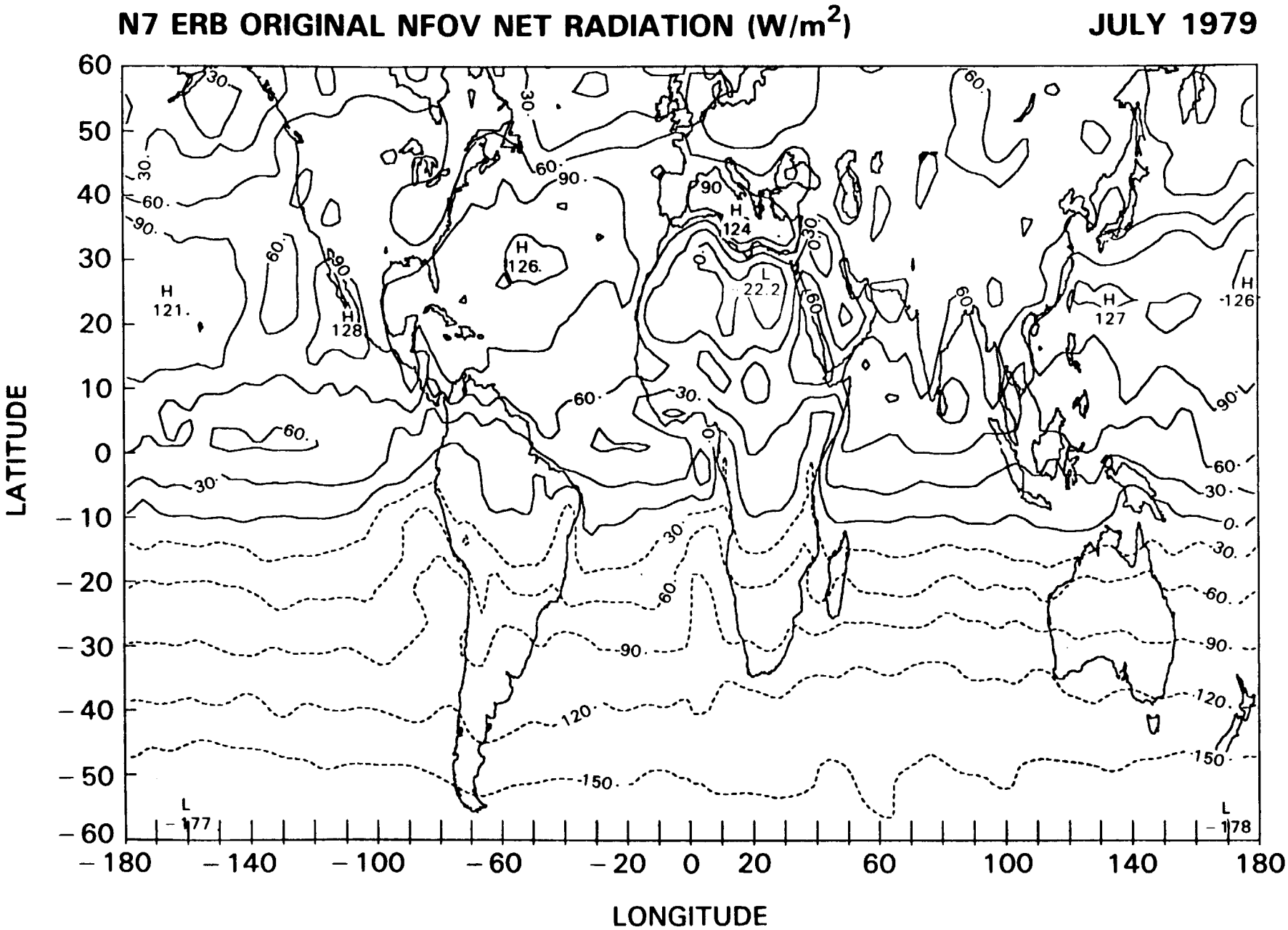
N7 ERB ORIGINAL NFOV NET RADIATION (W/m²)
JULY 1979
LATITUDE
LONGITUDE
60
50
40
30
20
10
0
-10
-20
-30
-40
-50
-60
-180
-140
-100
-60
-20
0
20
60
100
140
180
H 121.
H 128
H 126.
H 124
L 22.2
H 127
H 126
L 177
L 178
30.
60.
90.
120.
150.

Fig. 1b

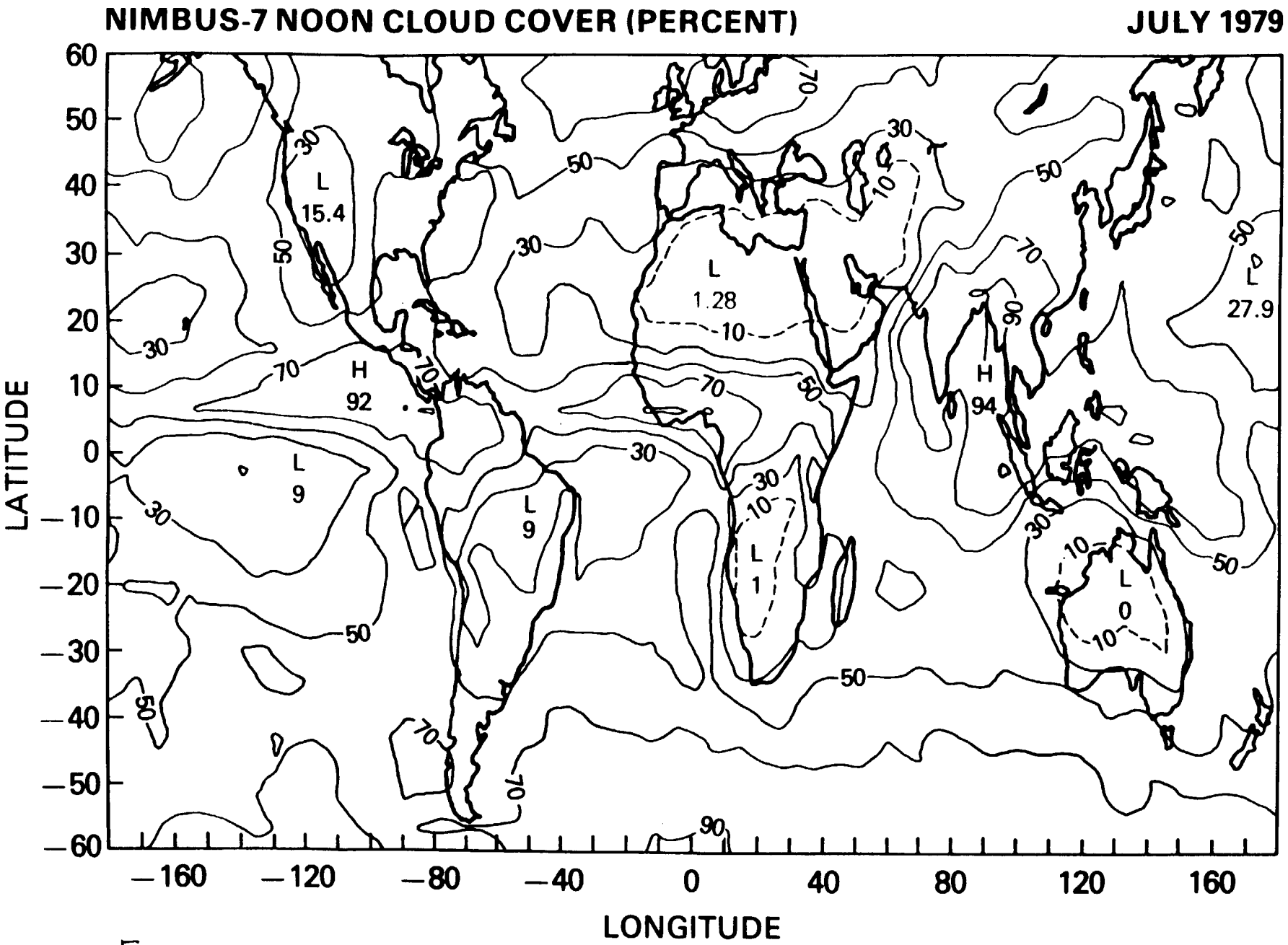
NIMBUS-7 NOON CLOUD COVER (PERCENT)
JULY 1979
LATITUDE
LONGITUDE
60
50
40
30
20
10
0
−10
−20
−30
−40
−50
−60
−160
−120
−80
−40
0
40
80
120
160
L
15.4
L
1.28
L
27.9
H
92
H
94
L
9
L
9
L
1
L
0
10
30
50
70
90

Fig. 2

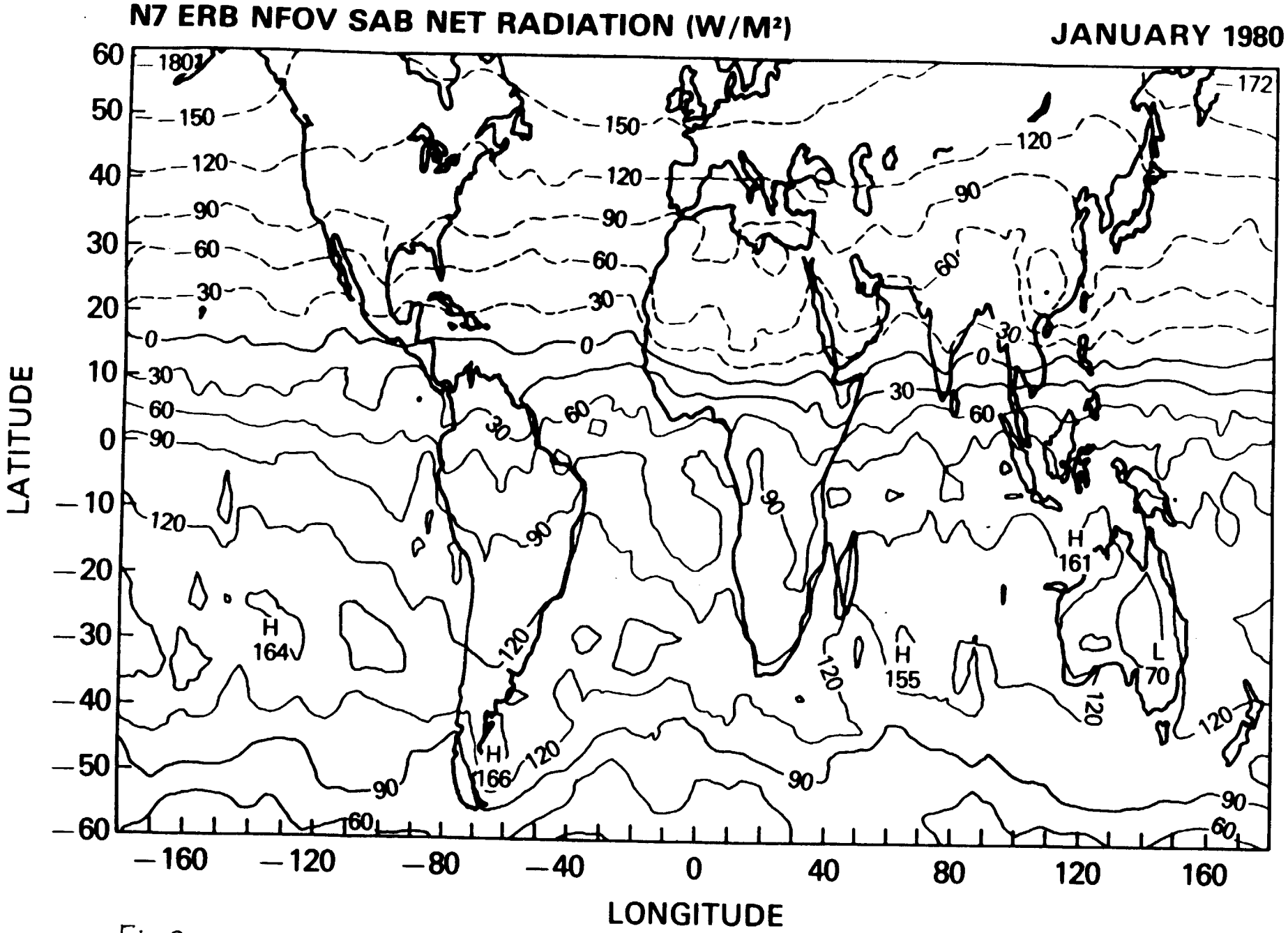
N7 ERB NFOV SAB NET RADIATION (W/M²)
JANUARY 1980
LATITUDE
LONGITUDE
60
50
40
30
20
10
0
−10
−20
−30
−40
−50
−60
−160
−120
−80
−40
0
40
80
120
160
180
150
120
90
60
30
0
−30
−60
−90
−120
172
H
164
H
166
H
155
H
161
L
70

Fig. 3

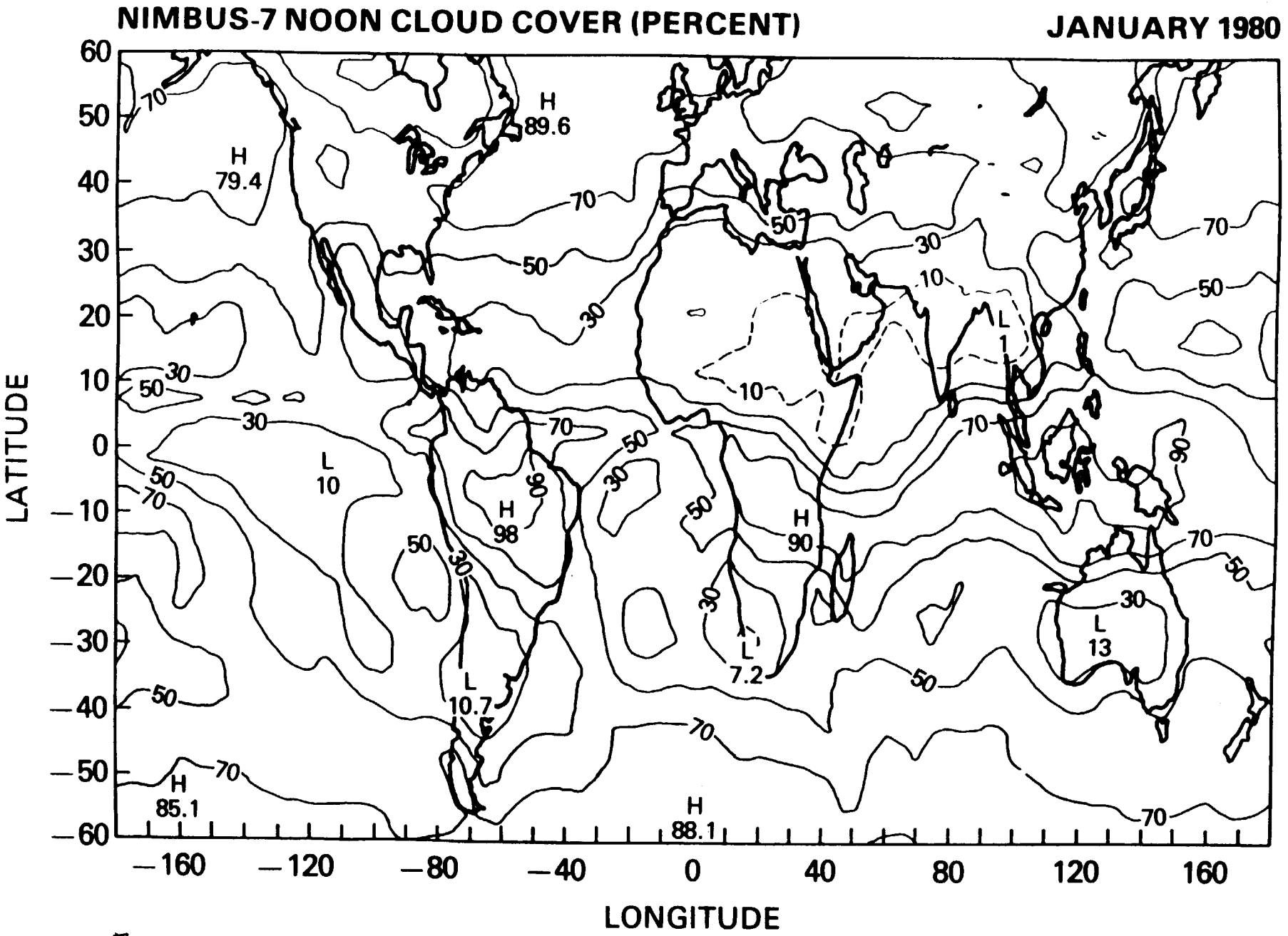
NIMBUS-7 NOON CLOUD COVER (PERCENT)
JANUARY 1980
LATITUDE
LONGITUDE
60
50
40
30
20
10
0
−10
−20
−30
−40
−50
−60
−160
−120
−80
−40
0
40
80
120
160
H 89.6
H 79.4
H 98
H 90
H 85.1
H 88.1
L 10
L 1
L 10.7
L 7.2
L 13
70
50
30
10

Fig. 4

STUDY REGIONS

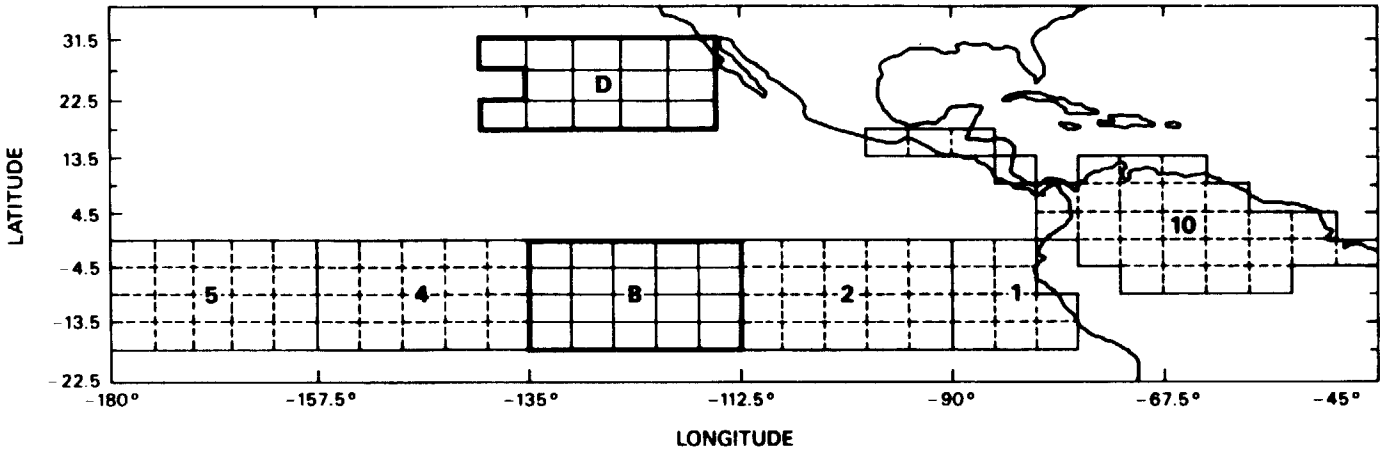

(A) EASTERN PACIFIC

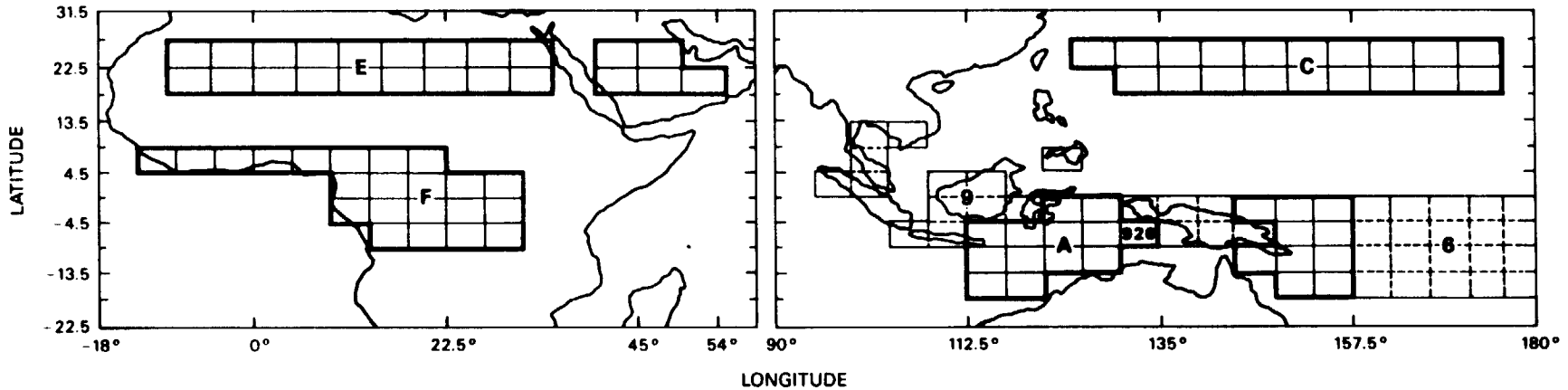

(C) AFRICA

(B) WESTERN PACIFIC

Fig. 5

POPULATIONS: JULY 1979

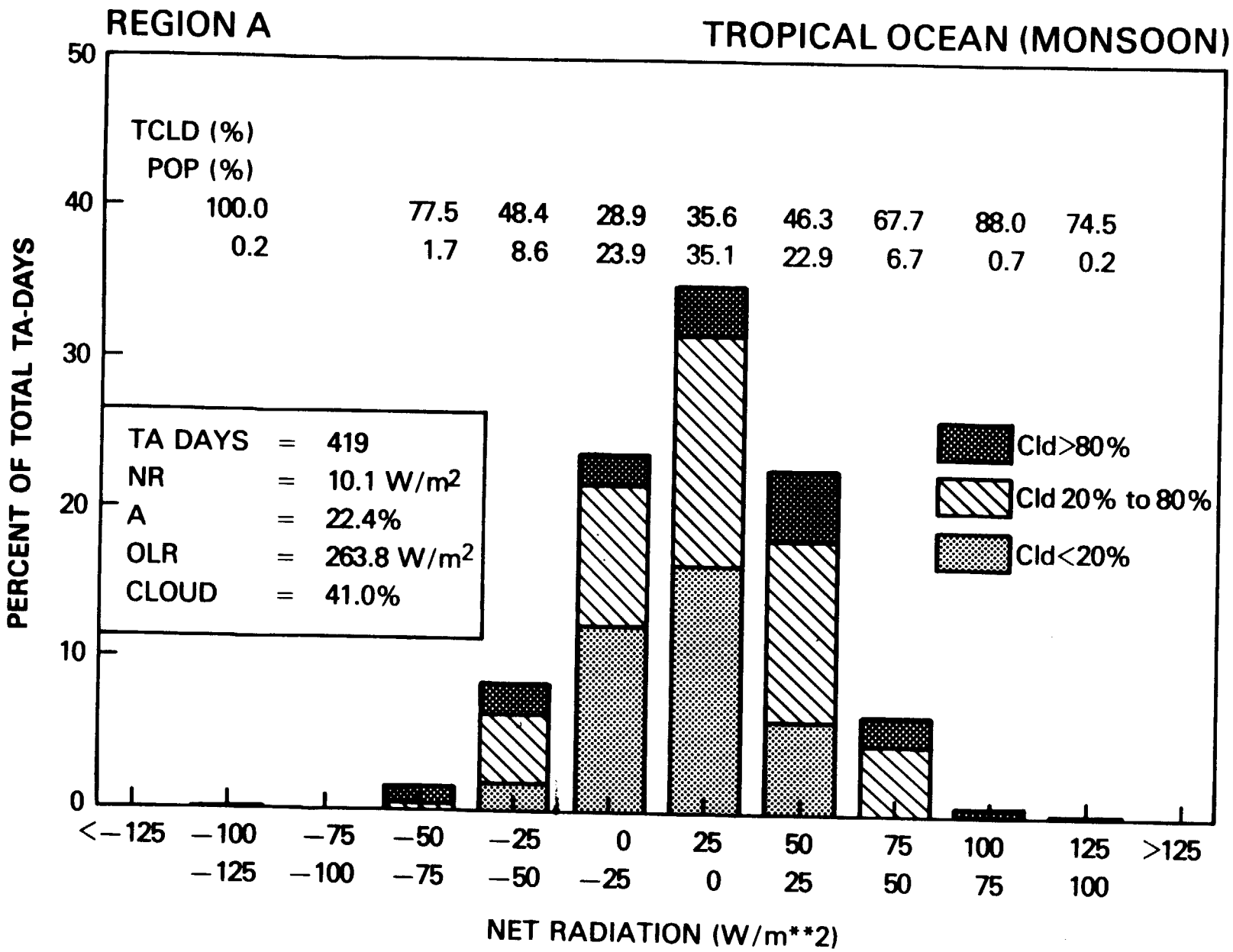

Fig. 6a

POPULATIONS: JULY 1979

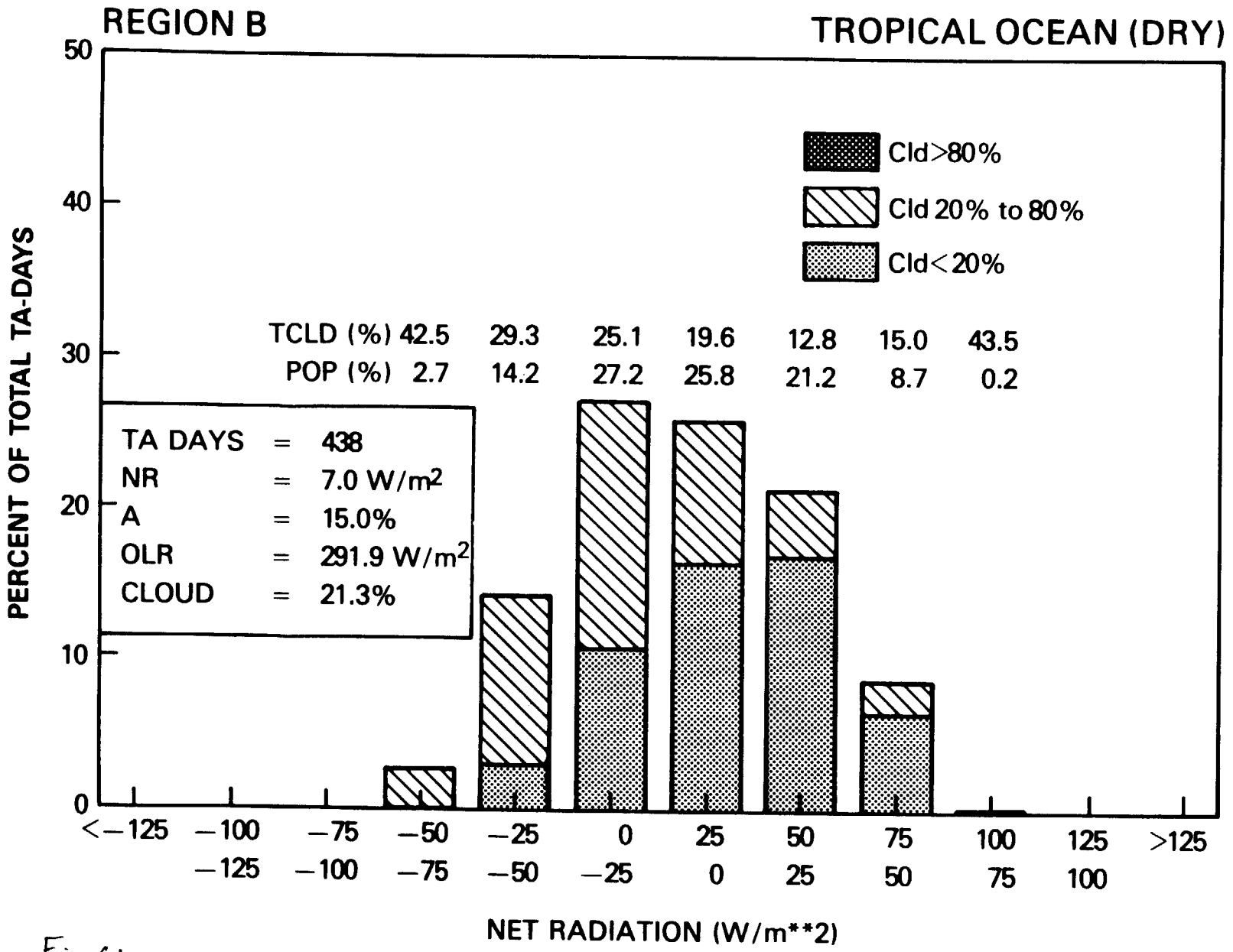

Fig. 6b

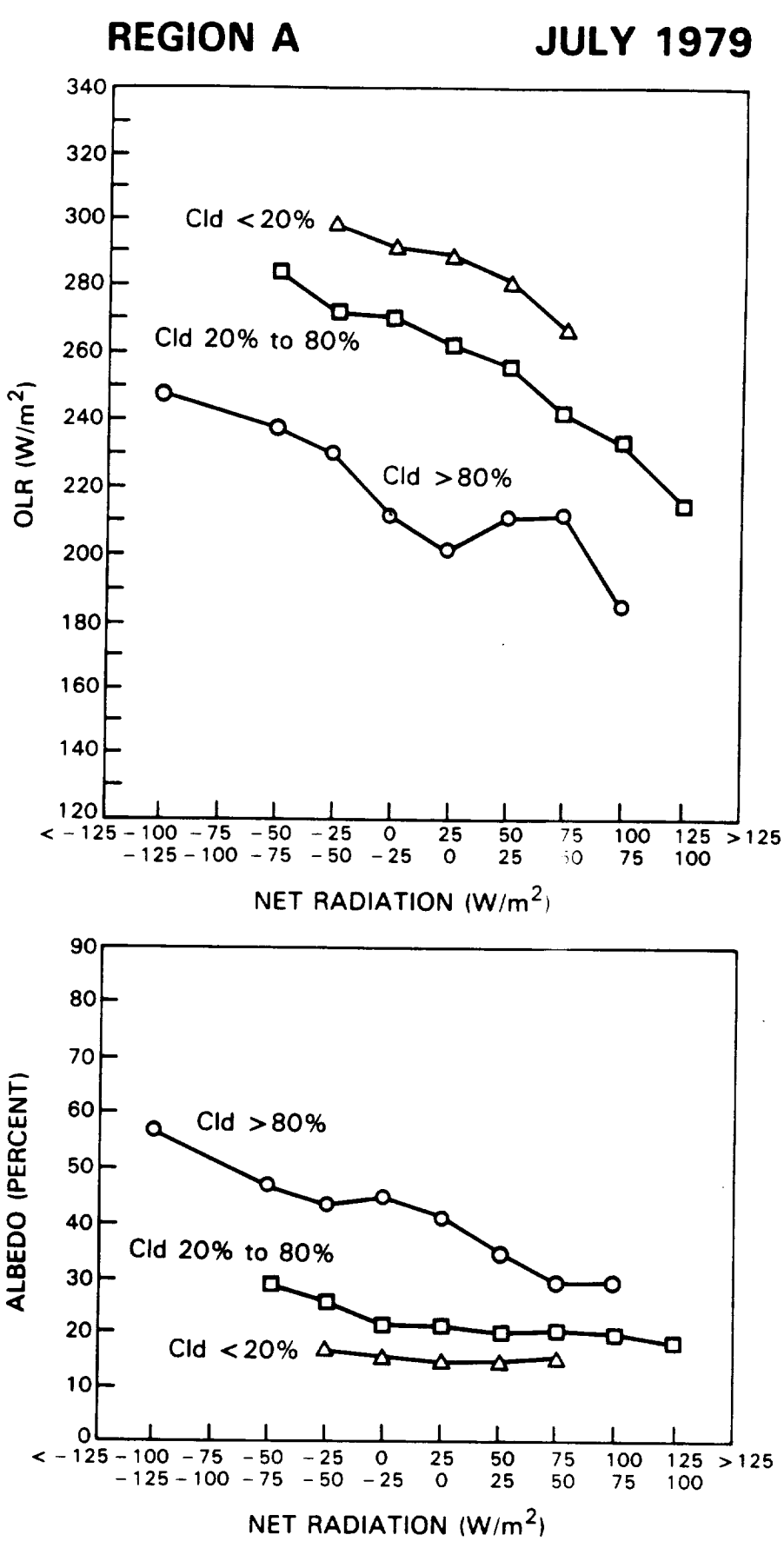
REGION A
JULY 1979
OLR (W/m²)
340
320
300
280
260
240
220
200
180
160
140
120
Cld < 20%
Cld 20% to 80%
Cld > 80%
< -125 -125 -100 -100 -75 -75 -50 -50 -25 -25 0 0 25 25 50 50 75 75 100 100 125 >125
NET RADIATION (W/m²)
ALBEDO (PERCENT)
90
80
70
60
50
40
30
20
10
0
Cld > 80%
Cld 20% to 80%
Cld < 20%
< -125 -125 -100 -100 -75 -75 -50 -50 -25 -25 0 0 25 25 50 50 75 75 100 100 125 >125
NET RADIATION (W/m²)

Fig. 7a

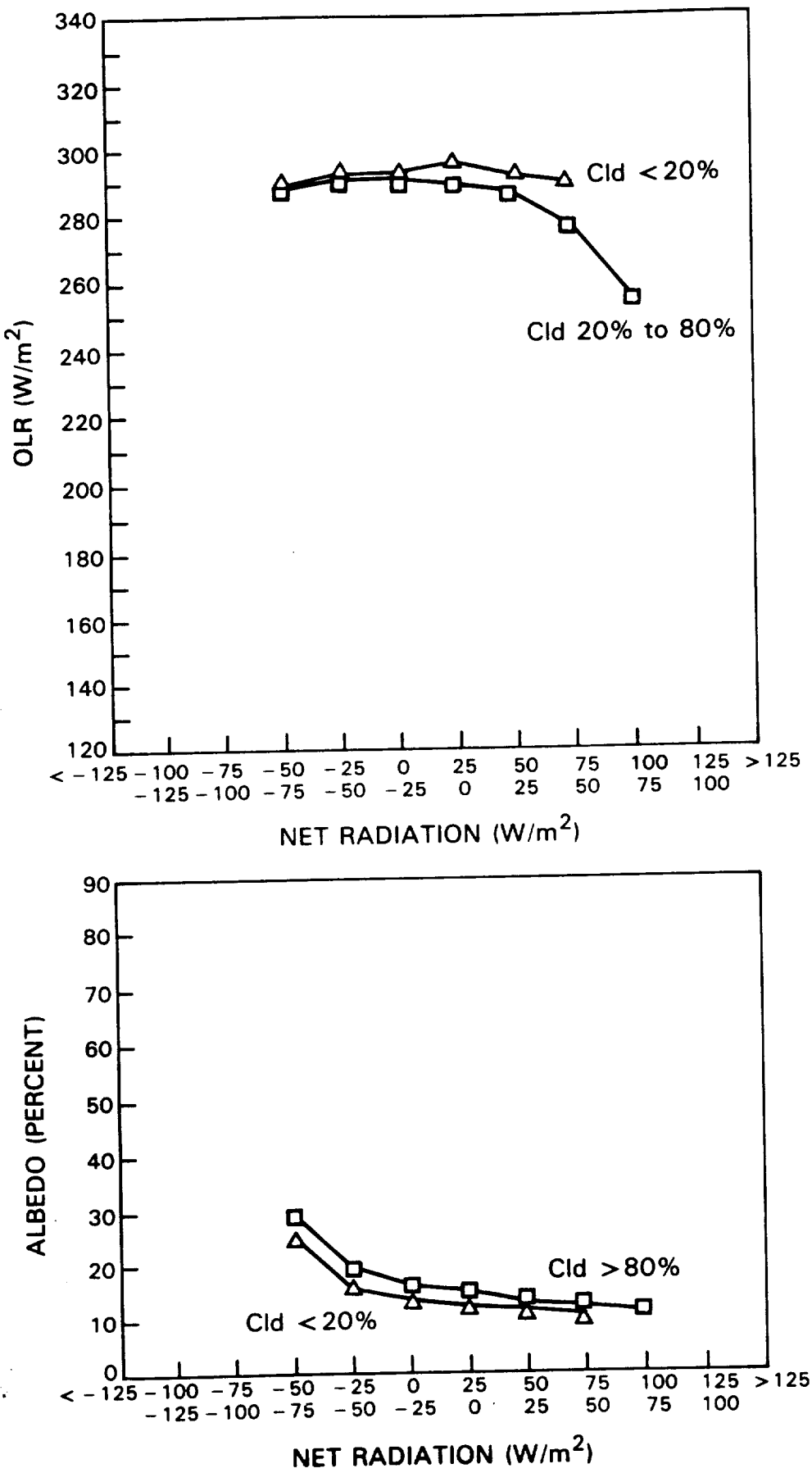
REGION B
JULY 1979
OLR (W/m2)
340
320
300
280
260
240
220
200
180
160
140
120
Cld < 20%
Cld 20% to 80%
< -125 -125 -100 -100 -75 -75 -50 -50 -25 -25 0 0 25 25 50 50 75 75 100 100 125 >125
NET RADIATION (W/m2)
ALBEDO (PERCENT)
90
80
70
60
50
40
30
20
10
0
Cld > 80%
Cld < 20%
< -125 -125 -100 -100 -75 -75 -50 -50 -25 -25 0 0 25 25 50 50 75 75 100 100 125 >125
NET RADIATION (W/m2)

Fig. 7b

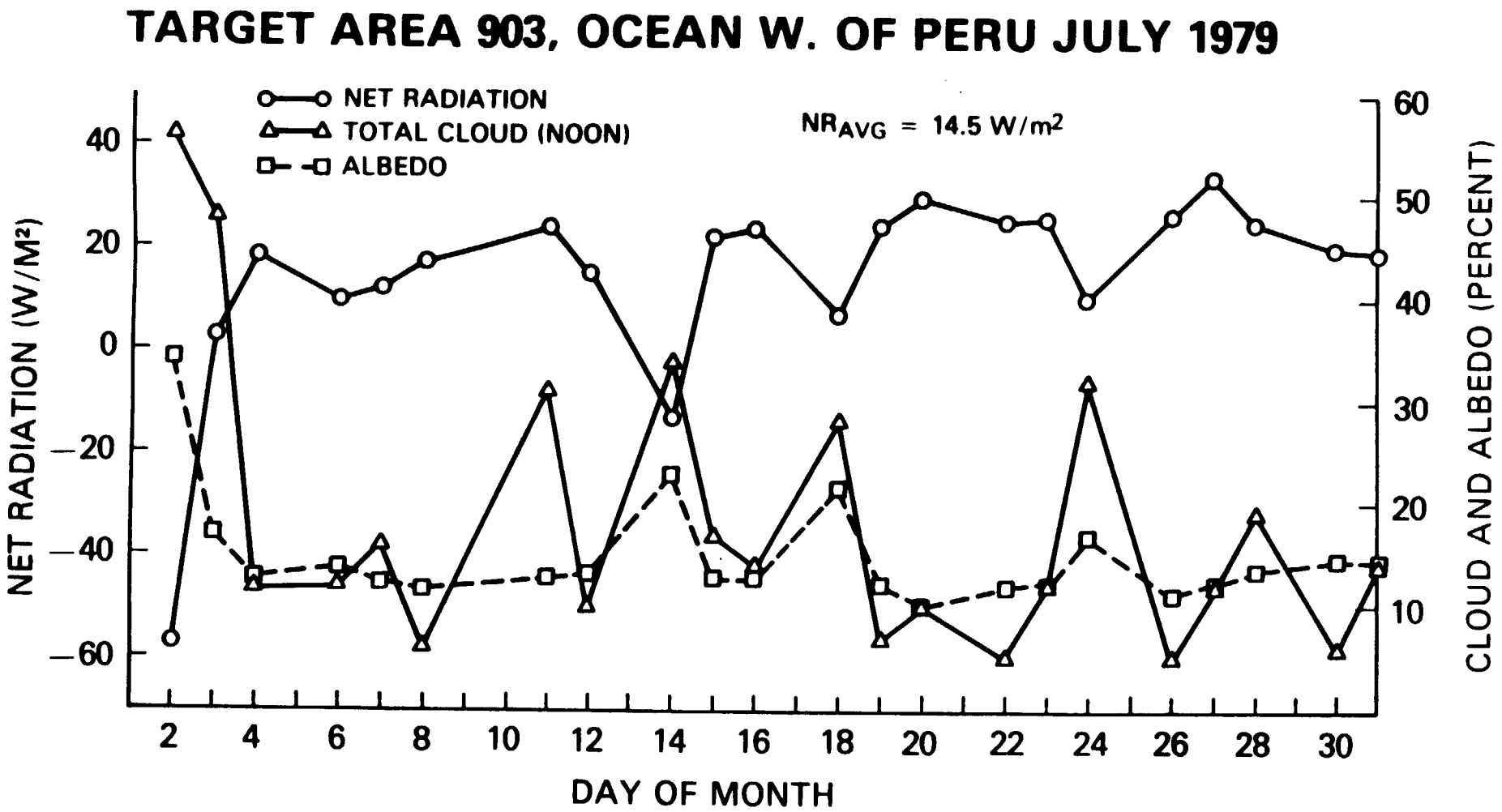
TARGET AREA 903, OCEAN W. OF PERU JULY 1979
NET RADIATION
TOTAL CLOUD (NOON)
ALBEDO
NR_AVG = 14.5 W/m2
NET RADIATION (W/M²)
CLOUD AND ALBEDO (PERCENT)
DAY OF MONTH
40
20
0
−20
−40
−60
60
50
40
30
20
10
2
4
6
8
10
12
14
16
18
20
22
24
26
28
30

Fig. 8

TARGET AREA 926, OCEAN N. OF AUSTRALIA JANUARY 1980

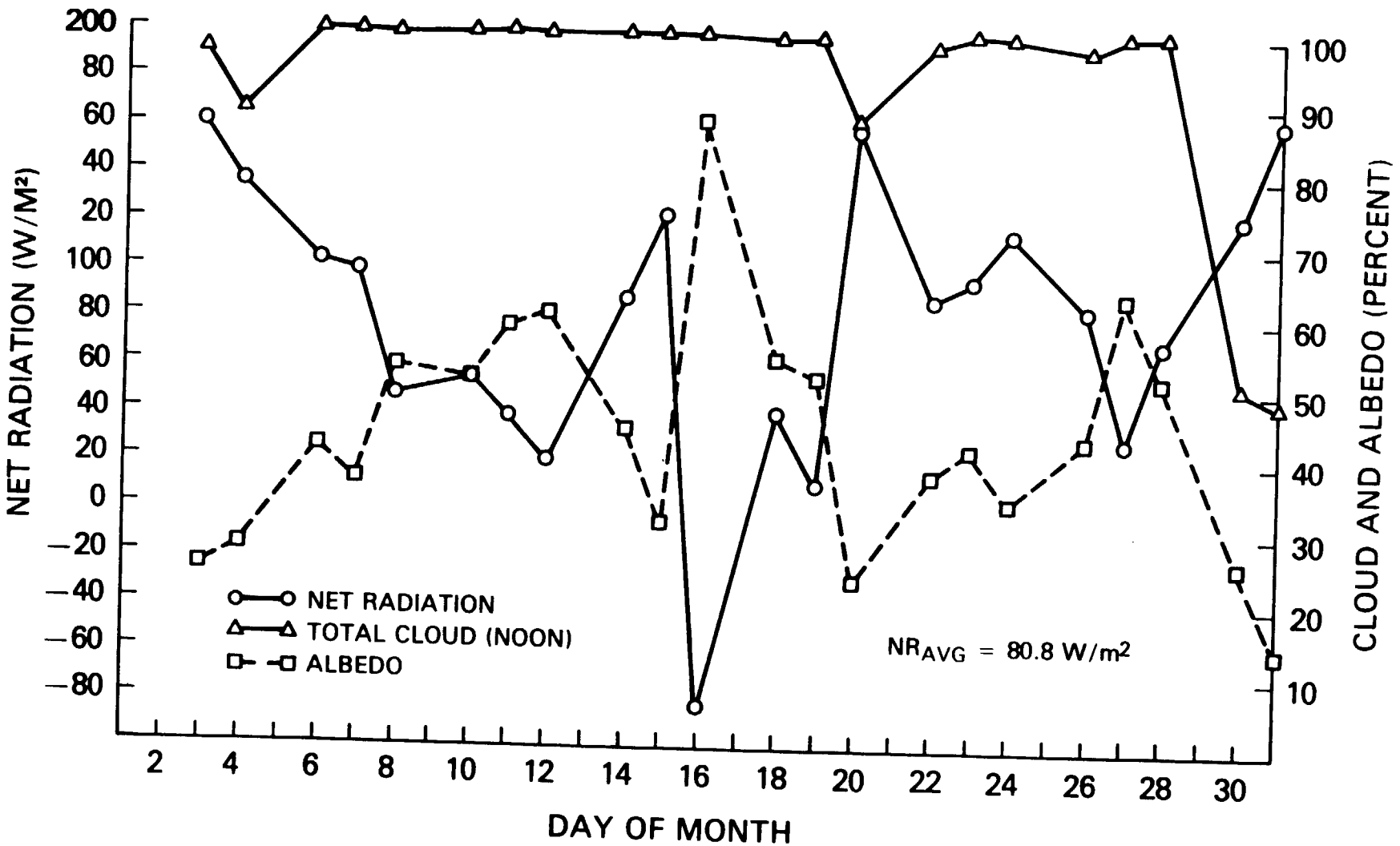

Fig. 9

POPULATIONS: JANUARY 1980

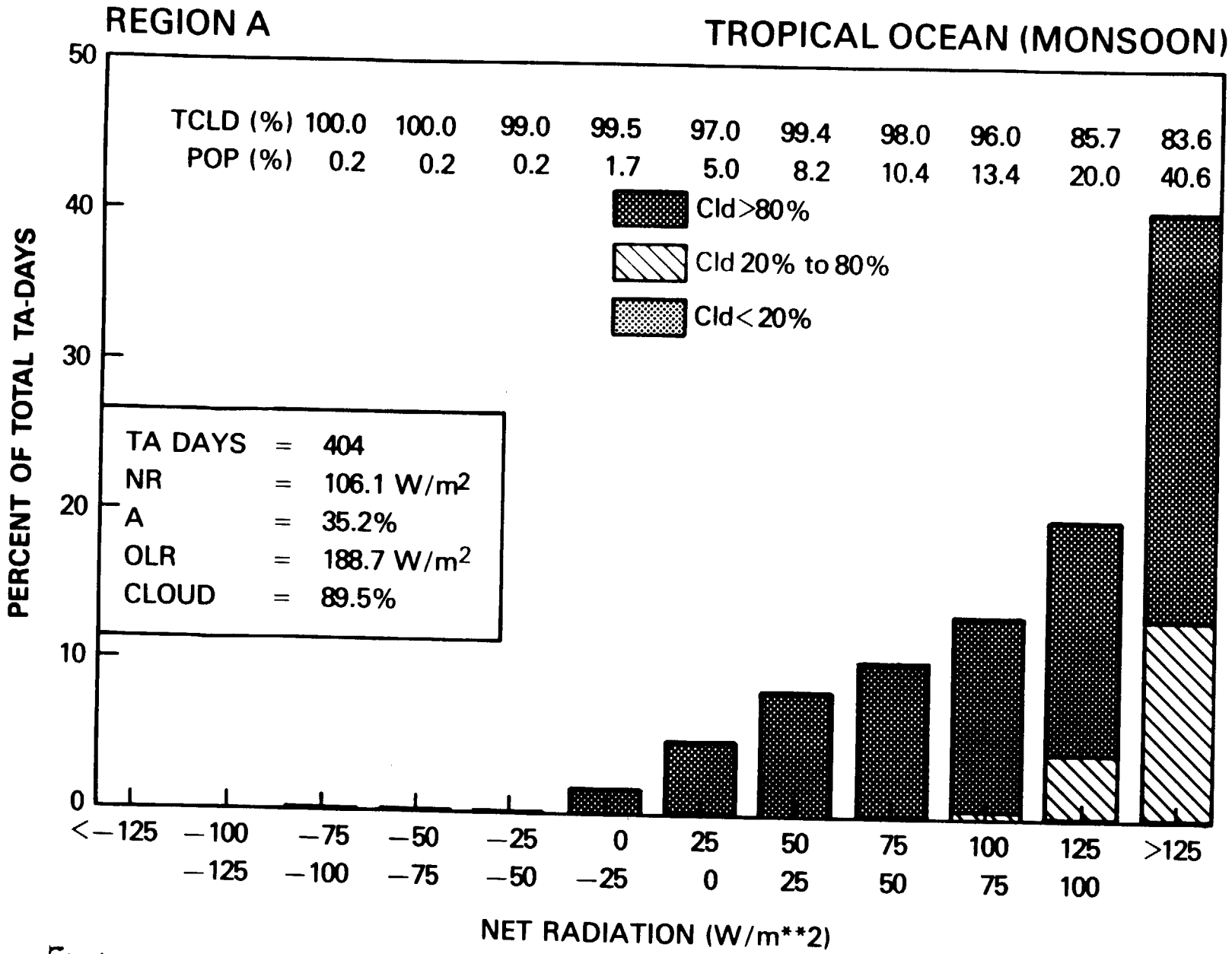

Fig. 10a

POPULATIONS: JANUARY 1980

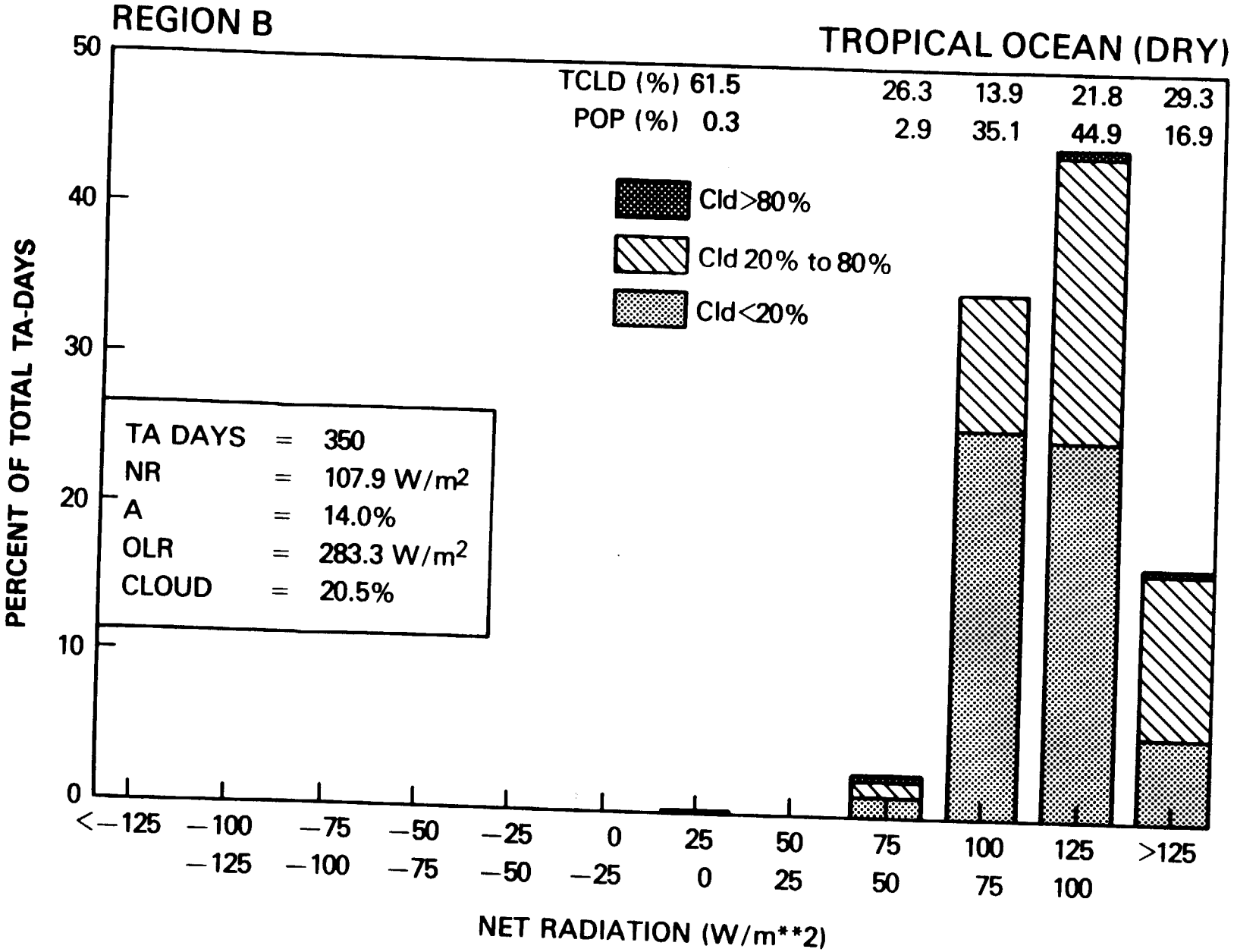

Fig 10b

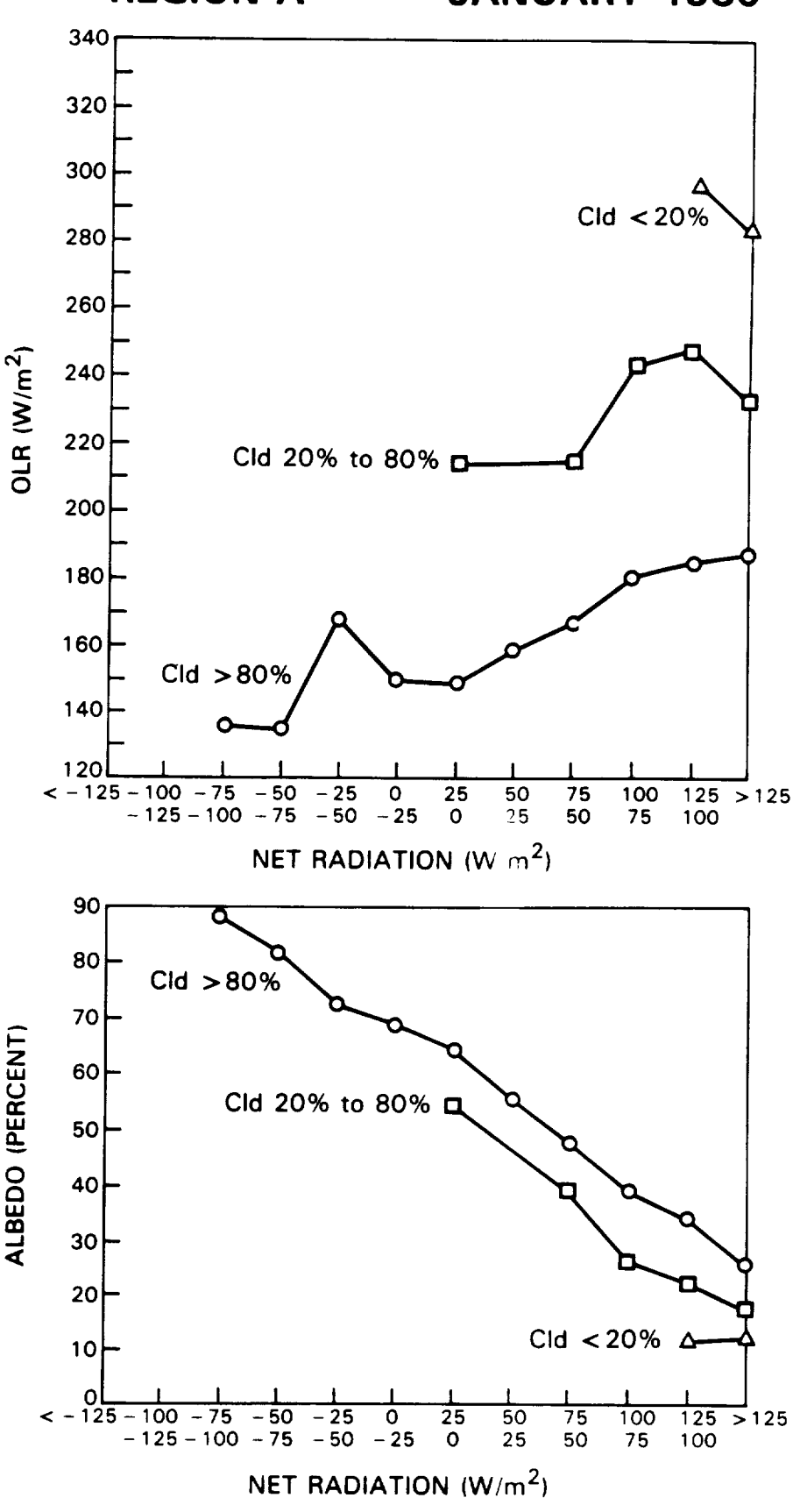
REGION A
JANUARY 1980
OLR (W/m²)
340
320
300
280
260
240
220
200
180
160
140
120
Cld < 20%
Cld 20% to 80%
Cld > 80%
< -125 -125 -100 -100 -75 -75 -50 -50 -25 -25 0 0 25 25 50 50 75 75 100 100 125 >125
NET RADIATION (W m²)
ALBEDO (PERCENT)
90
80
70
60
50
40
30
20
10
0
Cld > 80%
Cld 20% to 80%
Cld < 20%
< -125 -125 -100 -100 -75 -75 -50 -50 -25 -25 0 0 25 25 50 50 75 75 100 100 125 >125
NET RADIATION (W/m²)

Fig. 11a

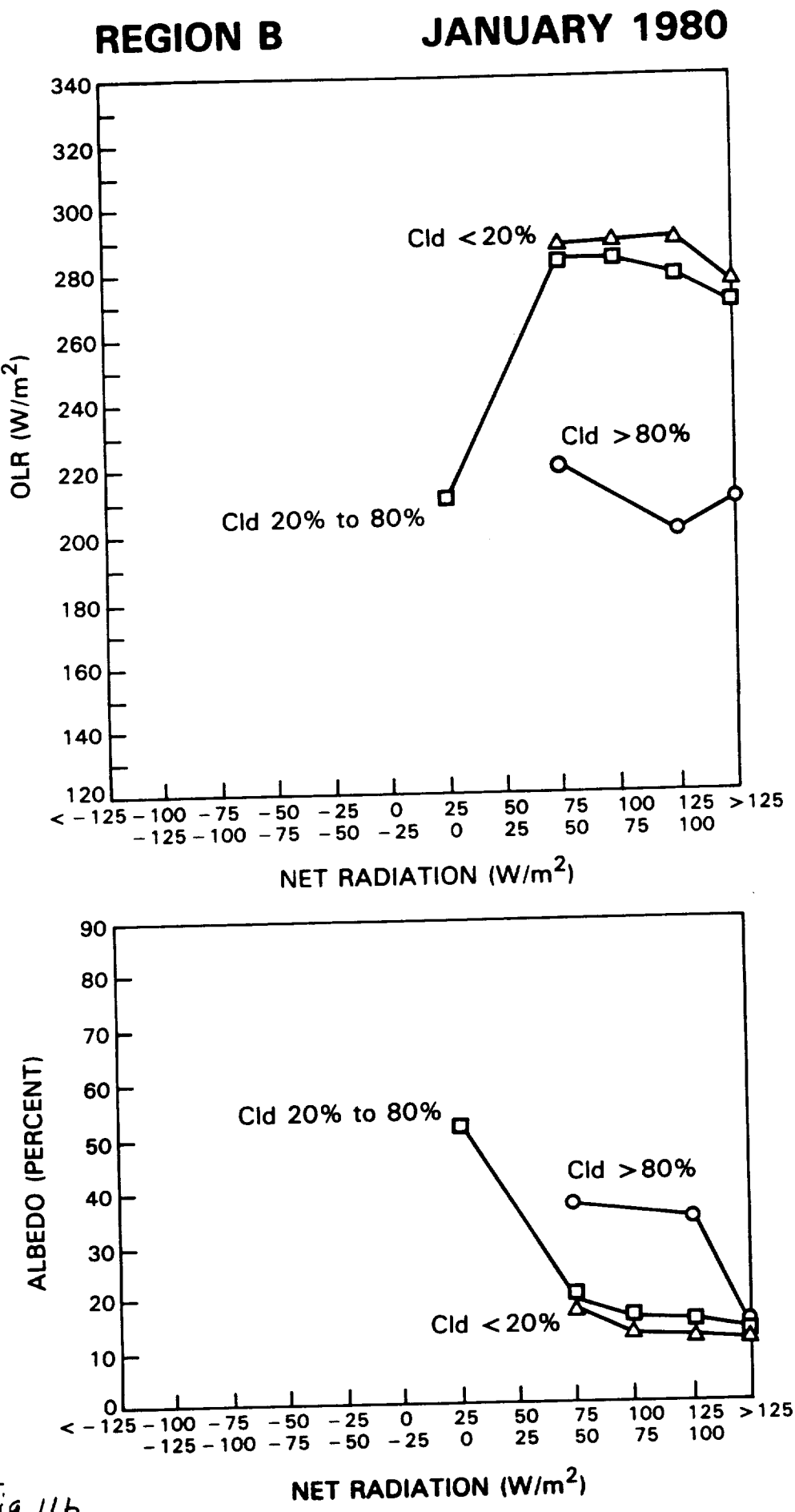
REGION B
JANUARY 1980
OLR (W/m2)
340
320
300
280
260
240
220
200
180
160
140
120
Cld <20%
Cld >80%
Cld 20% to 80%
< -125 -125 -100 -100 -75 -75 -50 -50 -25 -25 0 0 25 25 50 50 75 75 100 100 125 >125
NET RADIATION (W/m2)
ALBEDO (PERCENT)
90
80
70
60
50
40
30
20
10
0
Cld 20% to 80%
Cld >80%
Cld <20%
< -125 -125 -100 -100 -75 -75 -50 -50 -25 -25 0 0 25 25 50 50 75 75 100 100 125 >125
NET RADIATION (W/m2)

Fig. 11b

CLOUD TYPES , NOON; REGION A
JANUARY 1980

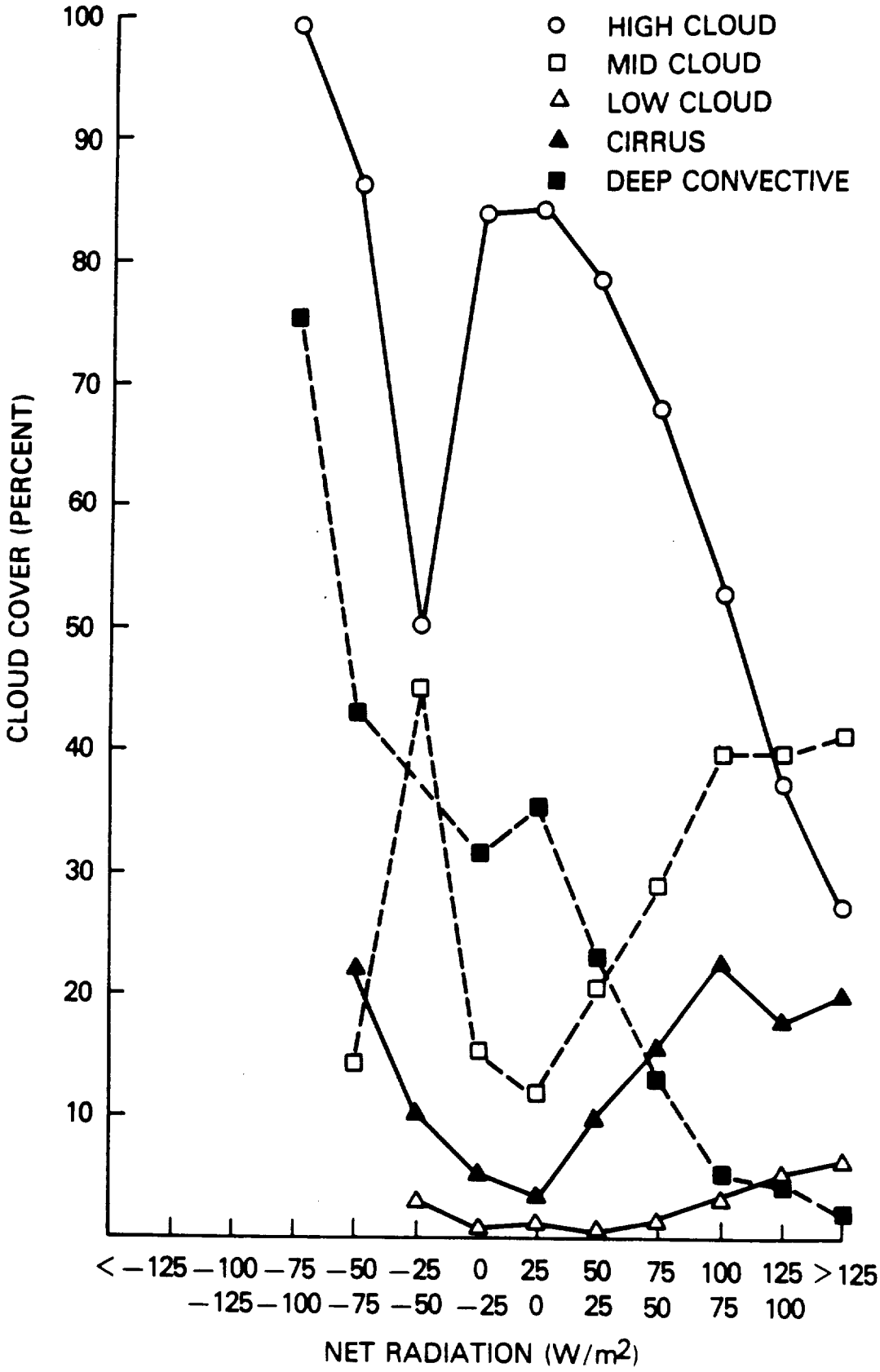

Fig. 12 a

CLOUD TYPES , NOON; REGION B
JANUARY 1980

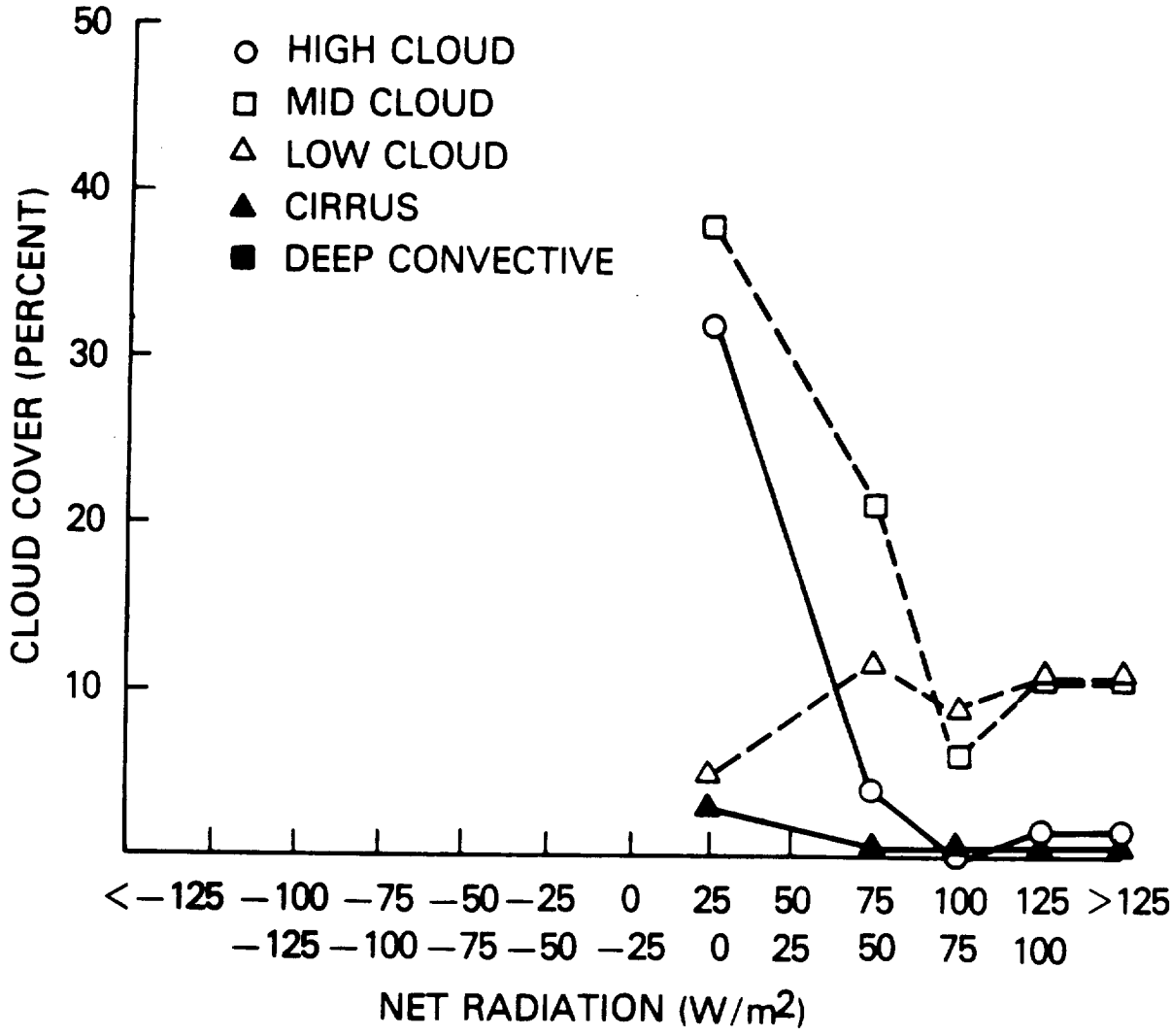

Fig. 12 b

POPULATIONS: JULY 1979

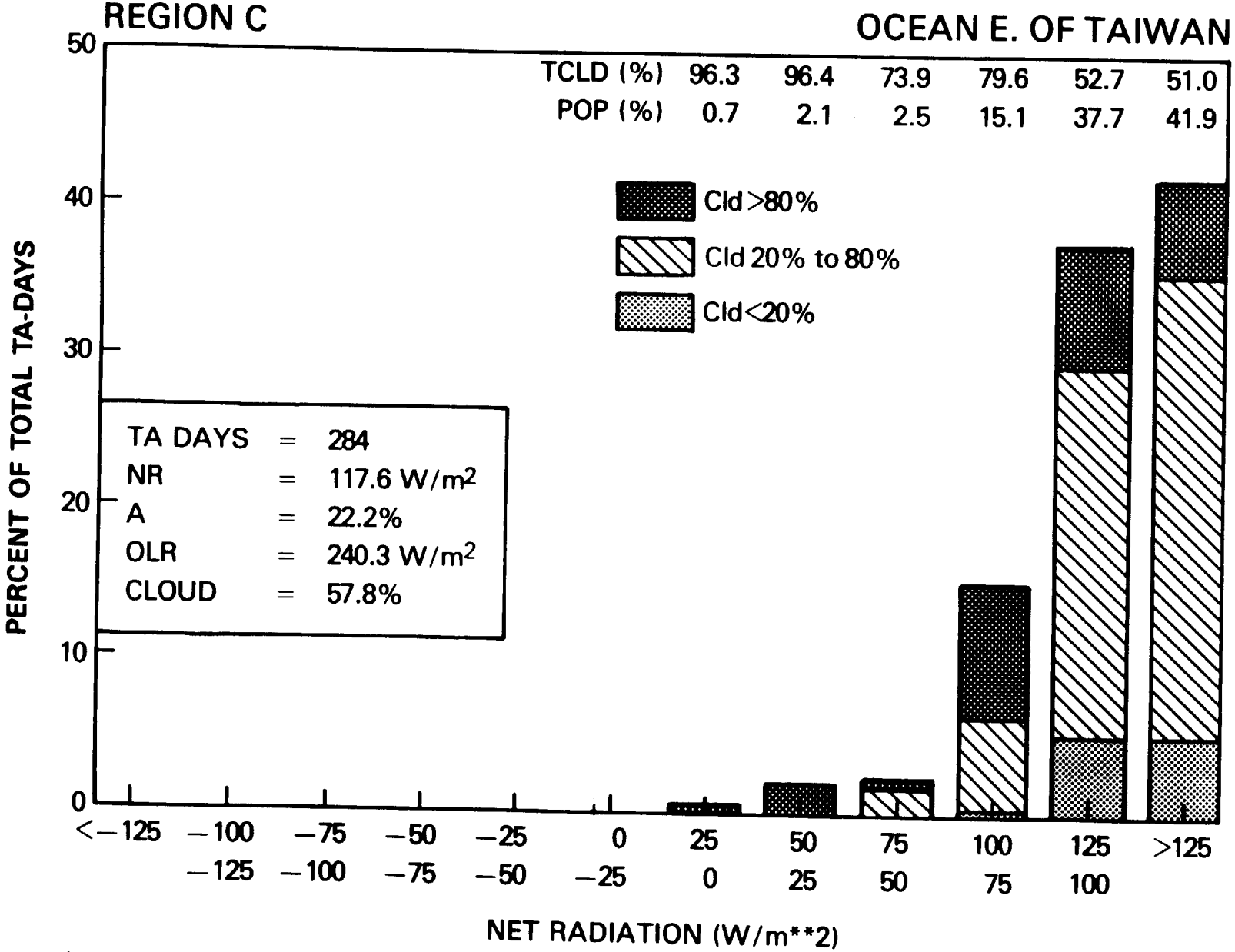

Fig.13a

POPULATIONS: JULY 1979

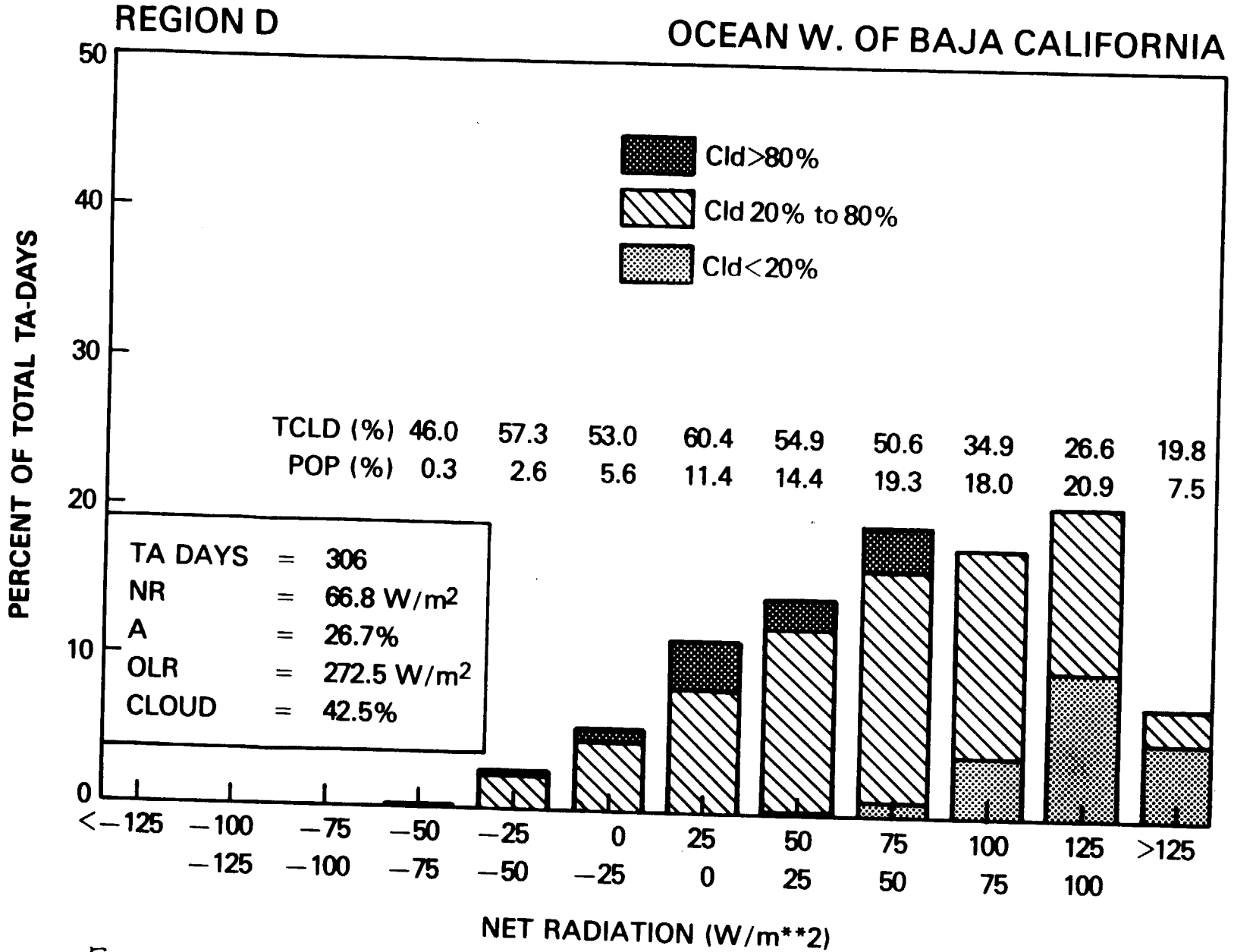

Fig. 13b

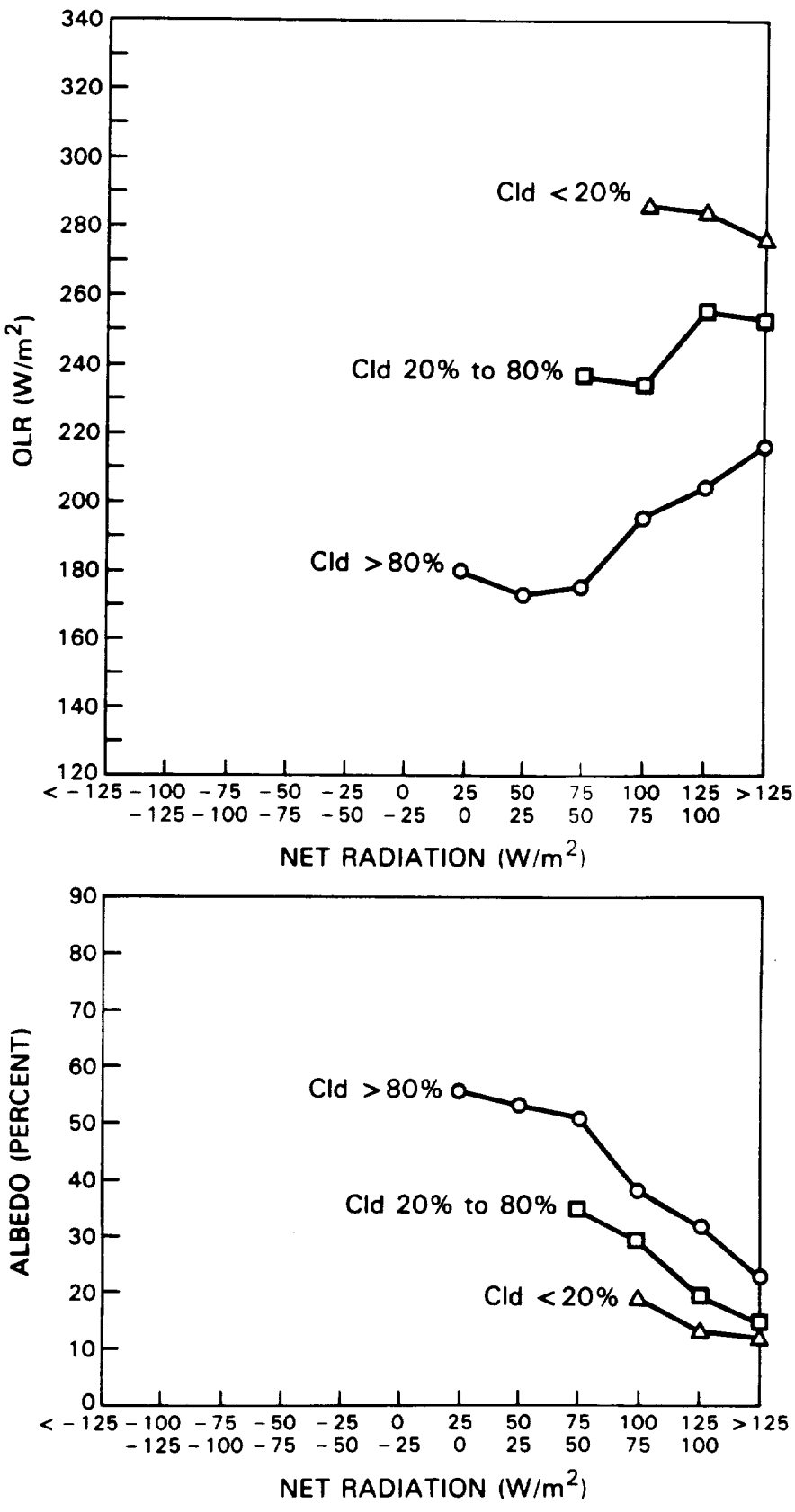
REGION C
JULY 1979
OLR (W/m2)
340
320
300
280
260
240
220
200
180
160
140
120
Cld < 20%
Cld 20% to 80%
Cld > 80%
< -125 -125 -100 -100 -75 -75 -50 -50 -25 -25 0 0 25 25 50 50 75 75 100 100 125 >125
NET RADIATION (W/m2)
ALBEDO (PERCENT)
90
80
70
60
50
40
30
20
10
0
Cld > 80%
Cld 20% to 80%
Cld < 20%
< -125 -125 -100 -100 -75 -75 -50 -50 -25 -25 0 0 25 25 50 50 75 75 100 100 125 >125
NET RADIATION (W/m2)

Fig. 14a

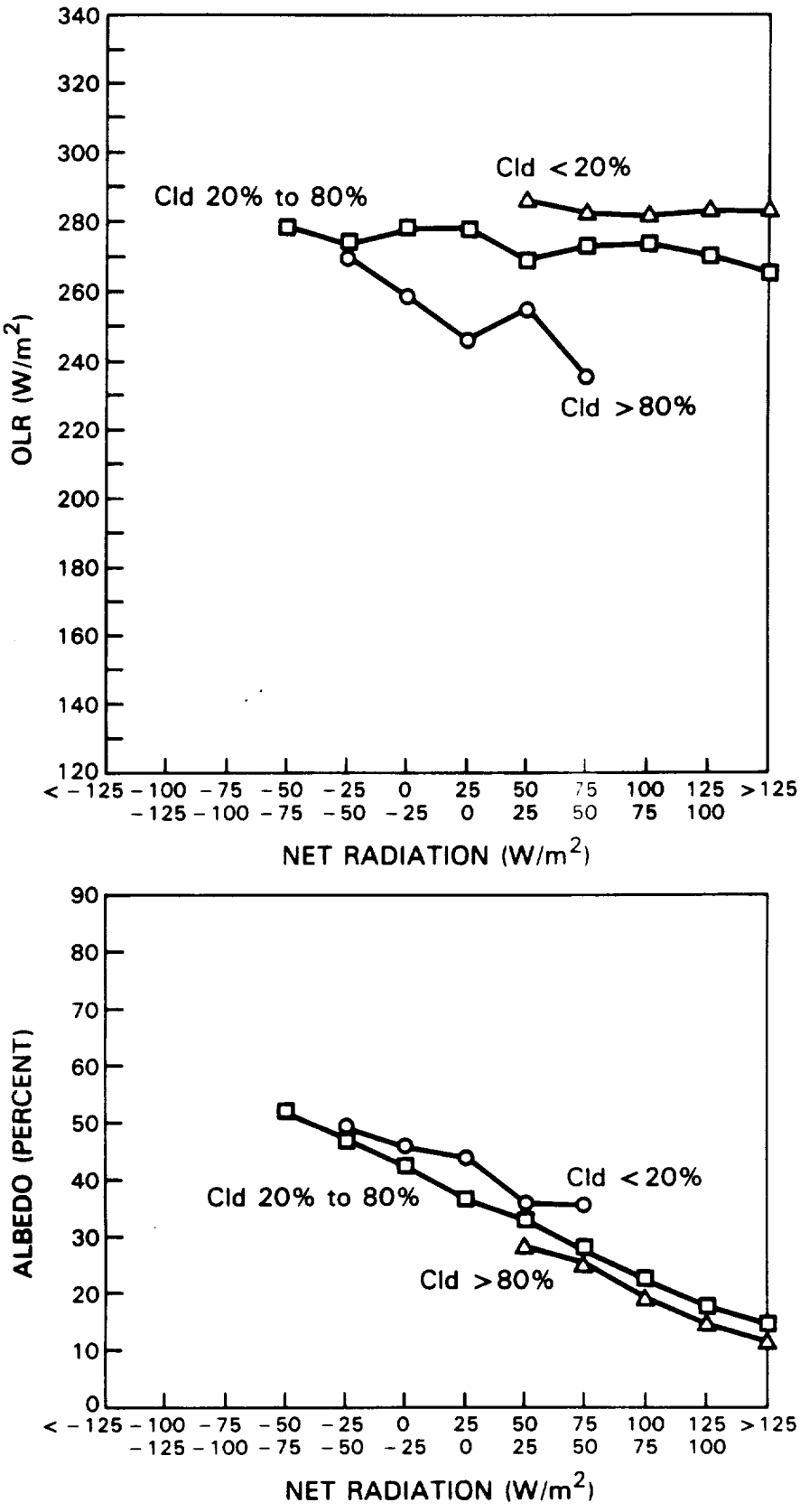
REGION D
JULY 1979
OLR (W/m²)
340
320
300
280
260
240
220
200
180
160
140
120
Cld < 20%
Cld 20% to 80%
Cld > 80%
< -125 -125 -100 -100 -75 -75 -50 -50 -25 -25 0 0 25 25 50 50 75 75 100 100 125 >125
NET RADIATION (W/m²)
ALBEDO (PERCENT)
90
80
70
60
50
40
30
20
10
0
Cld < 20%
Cld 20% to 80%
Cld > 80%
< -125 -125 -100 -100 -75 -75 -50 -50 -25 -25 0 0 25 25 50 50 75 75 100 100 125 >125
NET RADIATION (W/m²)

Fig. 14b

POPULATIONS: JULY 1979

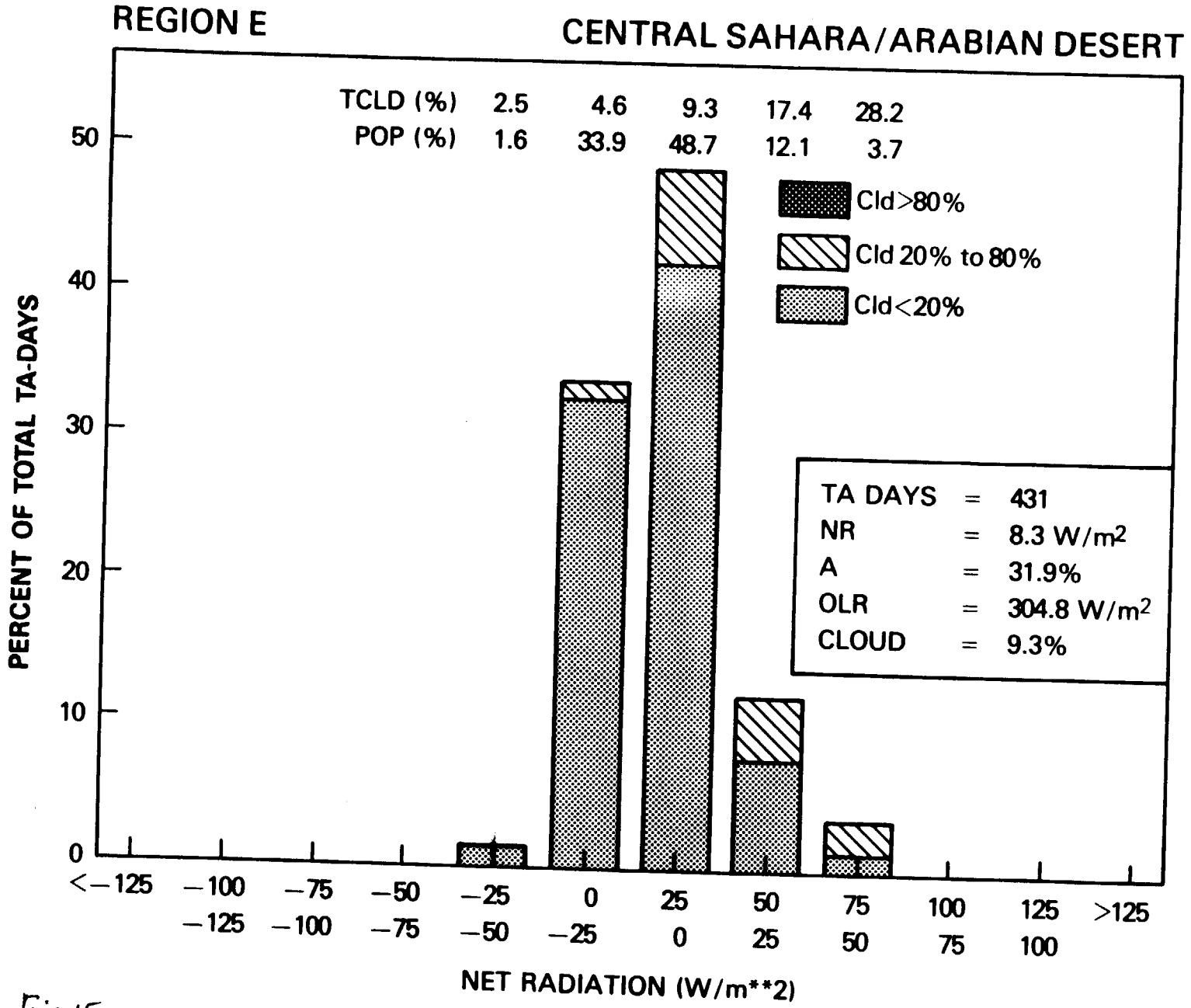

Fig. 15a

POPULATIONS: JULY 1979

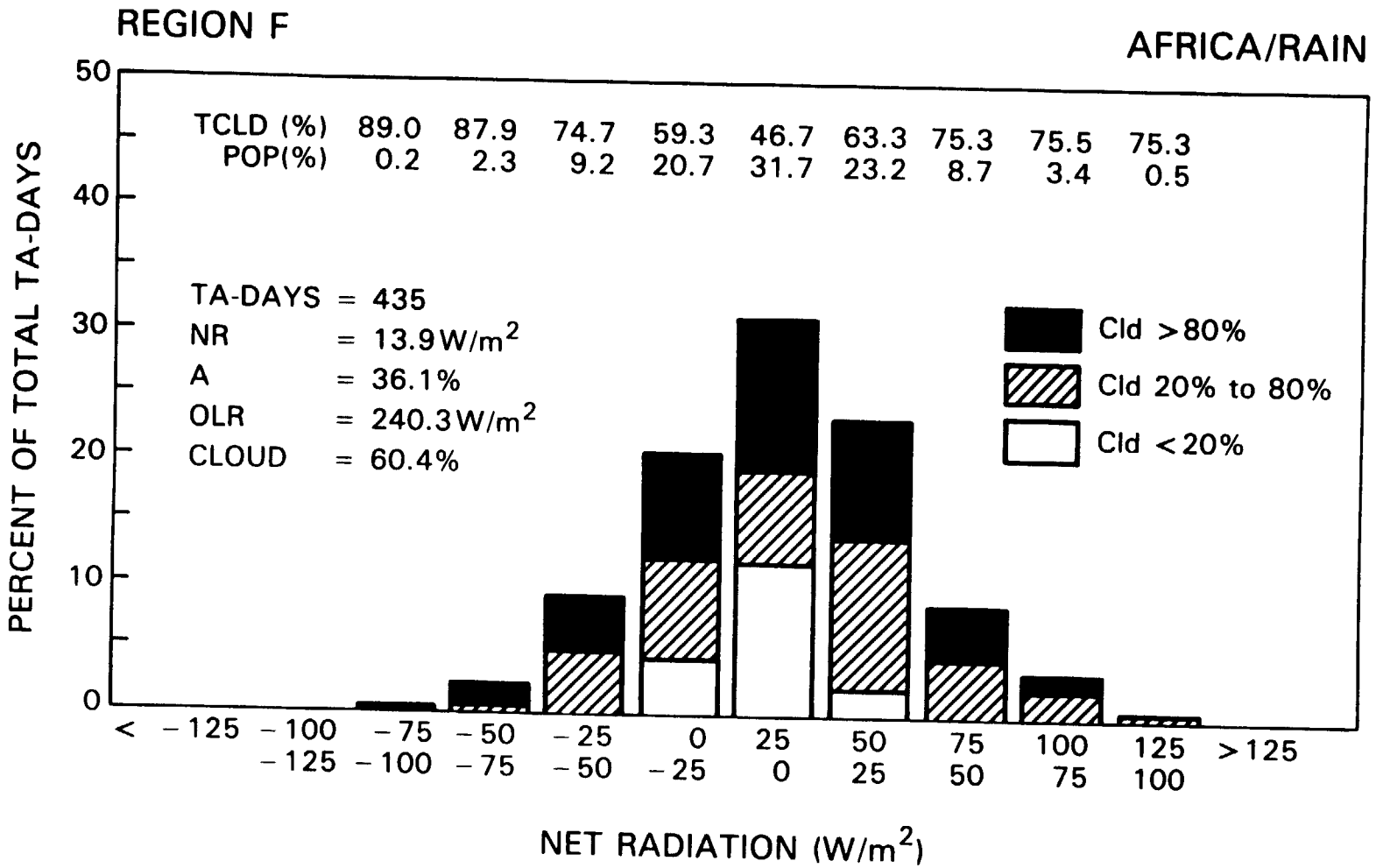

Fig 15b

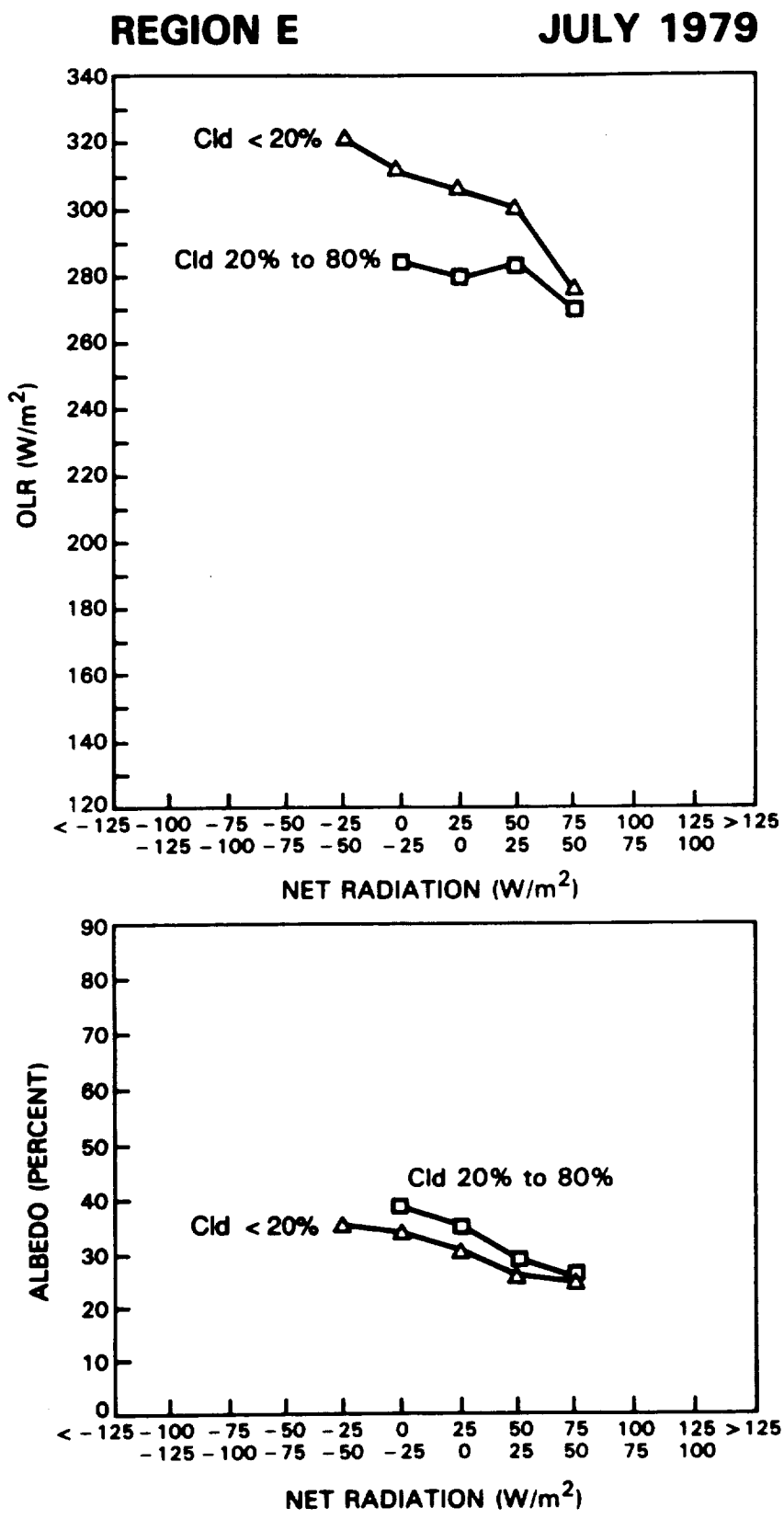
REGION E
JULY 1979
Cld < 20%
Cld 20% to 80%
OLR (W/m²)
340
320
300
280
260
240
220
200
180
160
140
120
< -125 -125 -100 -100 -75 -75 -50 -50 -25 -25 0 0 25 25 50 50 75 75 100 100 125 >125
NET RADIATION (W/m²)
ALBEDO (PERCENT)
90
80
70
60
50
40
30
20
10
0
Cld 20% to 80%
Cld < 20%
< -125 -125 -100 -100 -75 -75 -50 -50 -25 -25 0 0 25 25 50 50 75 75 100 100 125 >125
NET RADIATION (W/m²)

Fig 16a

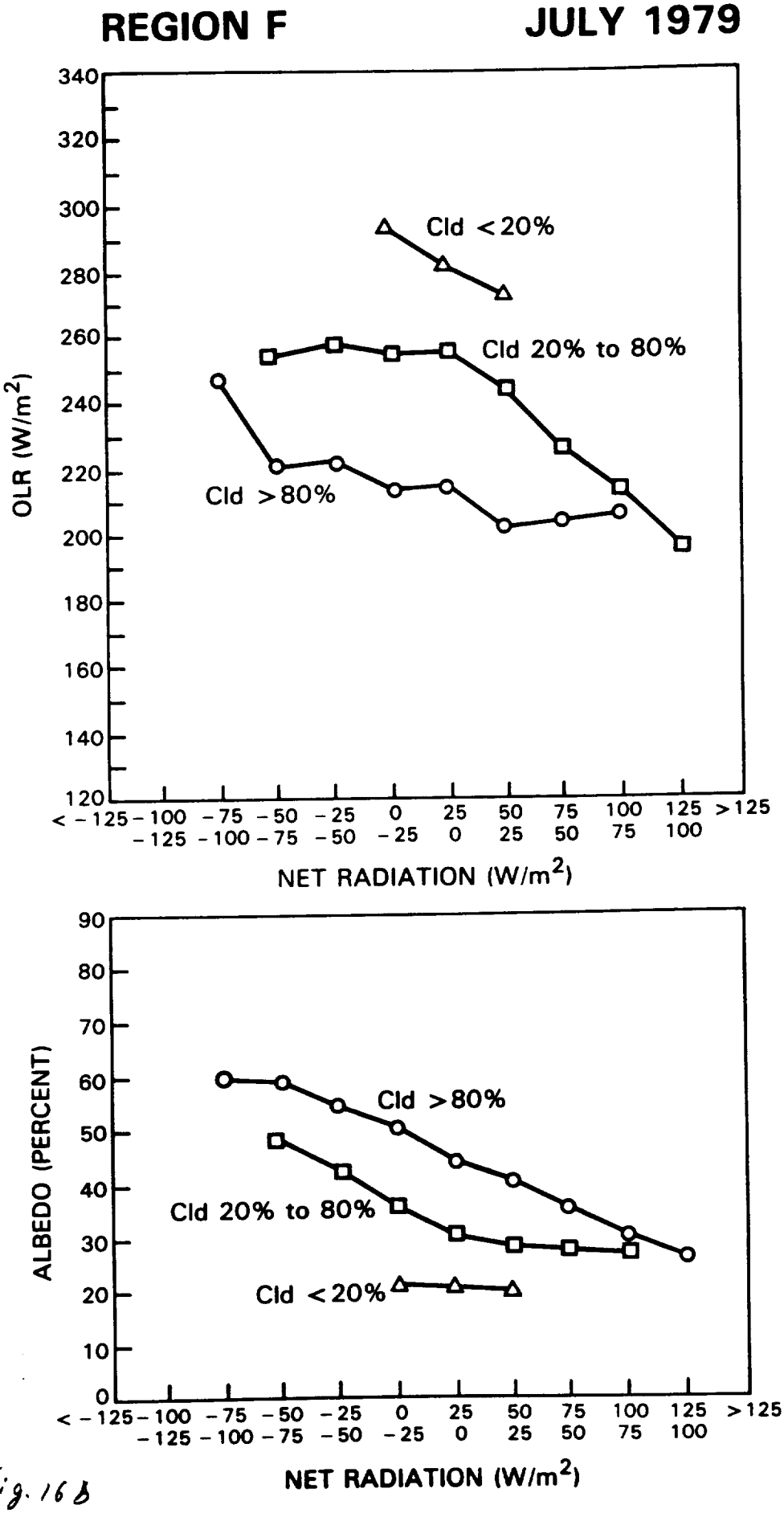
REGION F
JULY 1979
OLR (W/m²)
340
320
300
280
260
240
220
200
180
160
140
120
Cld < 20%
Cld 20% to 80%
Cld > 80%
< -125 -125
-100 -100
-75 -75
-50 -50
-25 -25
0 0
25 25
50 50
75 75
100 100
125 >125
NET RADIATION (W/m²)
ALBEDO (PERCENT)
90
80
70
60
50
40
30
20
10
0
Cld > 80%
Cld 20% to 80%
Cld < 20%
NET RADIATION (W/m²)

Fig. 16B

POPULATIONS: JANUARY 1980

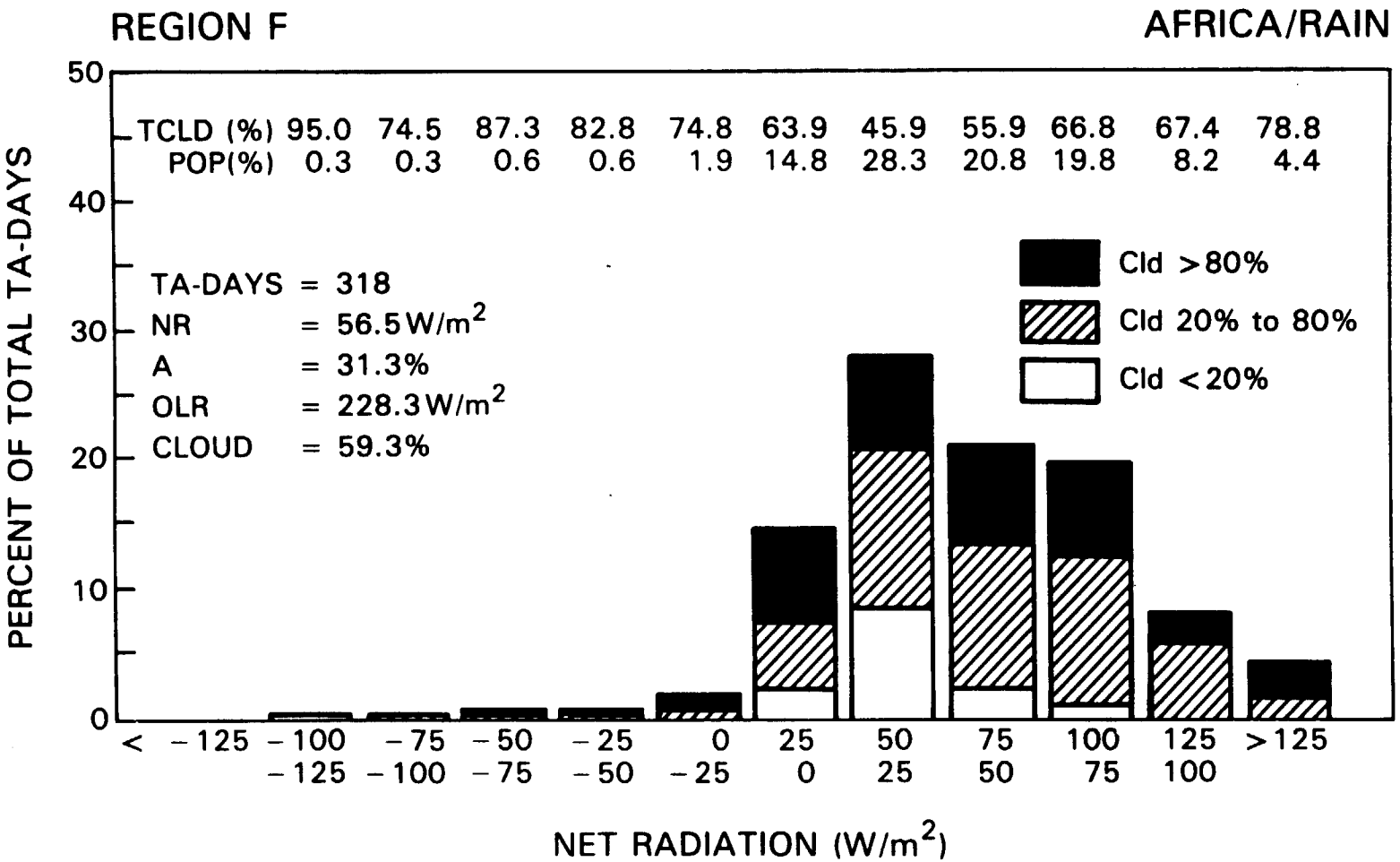

Fig. 17

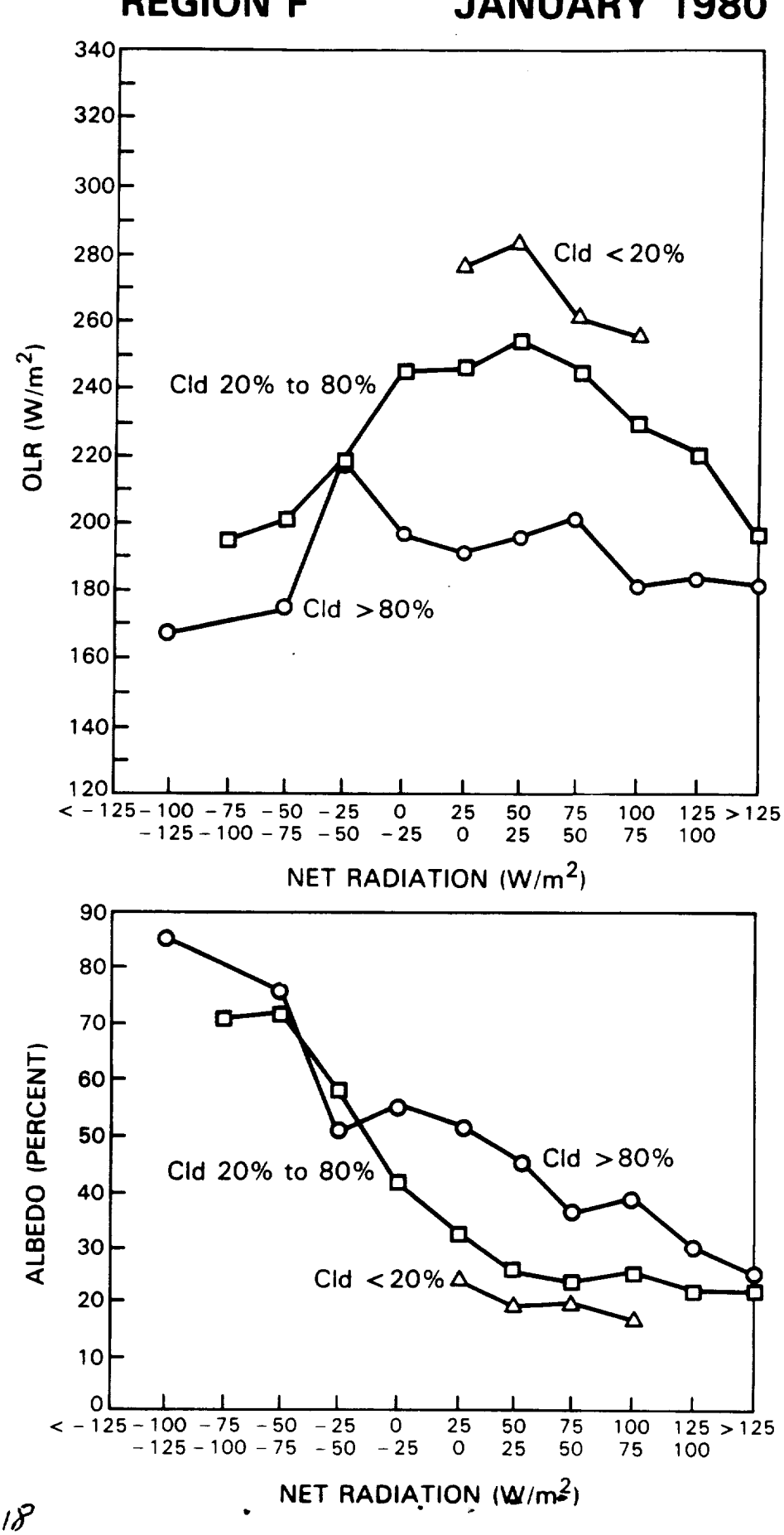
REGION F
JANUARY 1980
OLR (W/m²)
340
320
300
280
260
240
220
200
180
160
140
120
Cld < 20%
Cld 20% to 80%
Cld > 80%
< -125 -125 -100 -100 -75 -75 -50 -50 -25 -25 0 0 25 25 50 50 75 75 100 100 125 >125
NET RADIATION (W/m²)
ALBEDO (PERCENT)
90
80
70
60
50
40
30
20
10
0
Cld > 80%
Cld 20% to 80%
Cld < 20%
< -125 -125 -100 -100 -75 -75 -50 -50 -25 -25 0 0 25 25 50 50 75 75 100 100 125 >125
NET RADIATION (W/m²)

Fig. 18

OLR (NOON — MIDNIGHT) DIFFERENCE FOR STUDY AREAS A TO F, JULY

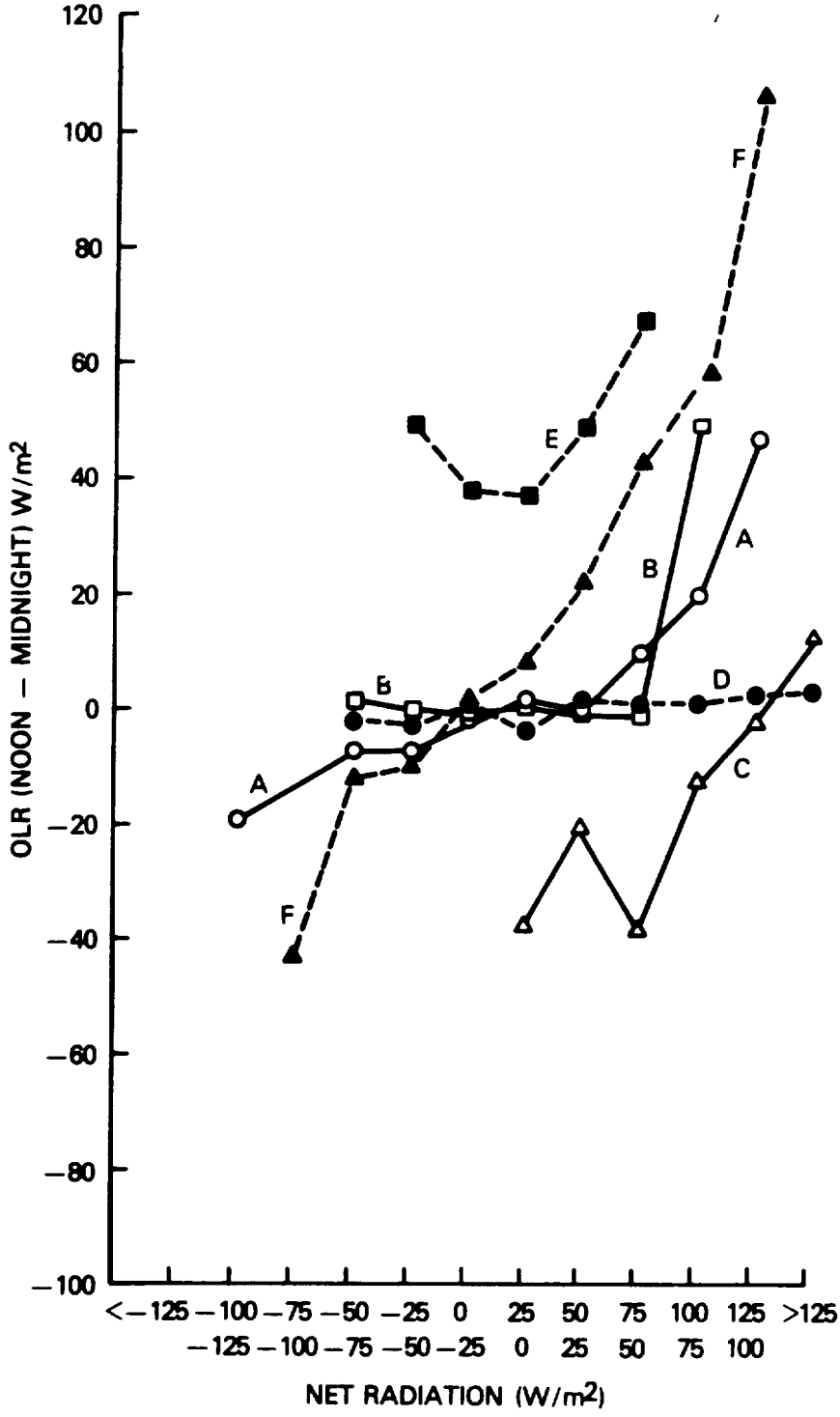

Fig. 19

OLR (NOON – MIDNIGHT) DIFFERENCE FOR STUDY AREAS A TO F, JANUARY

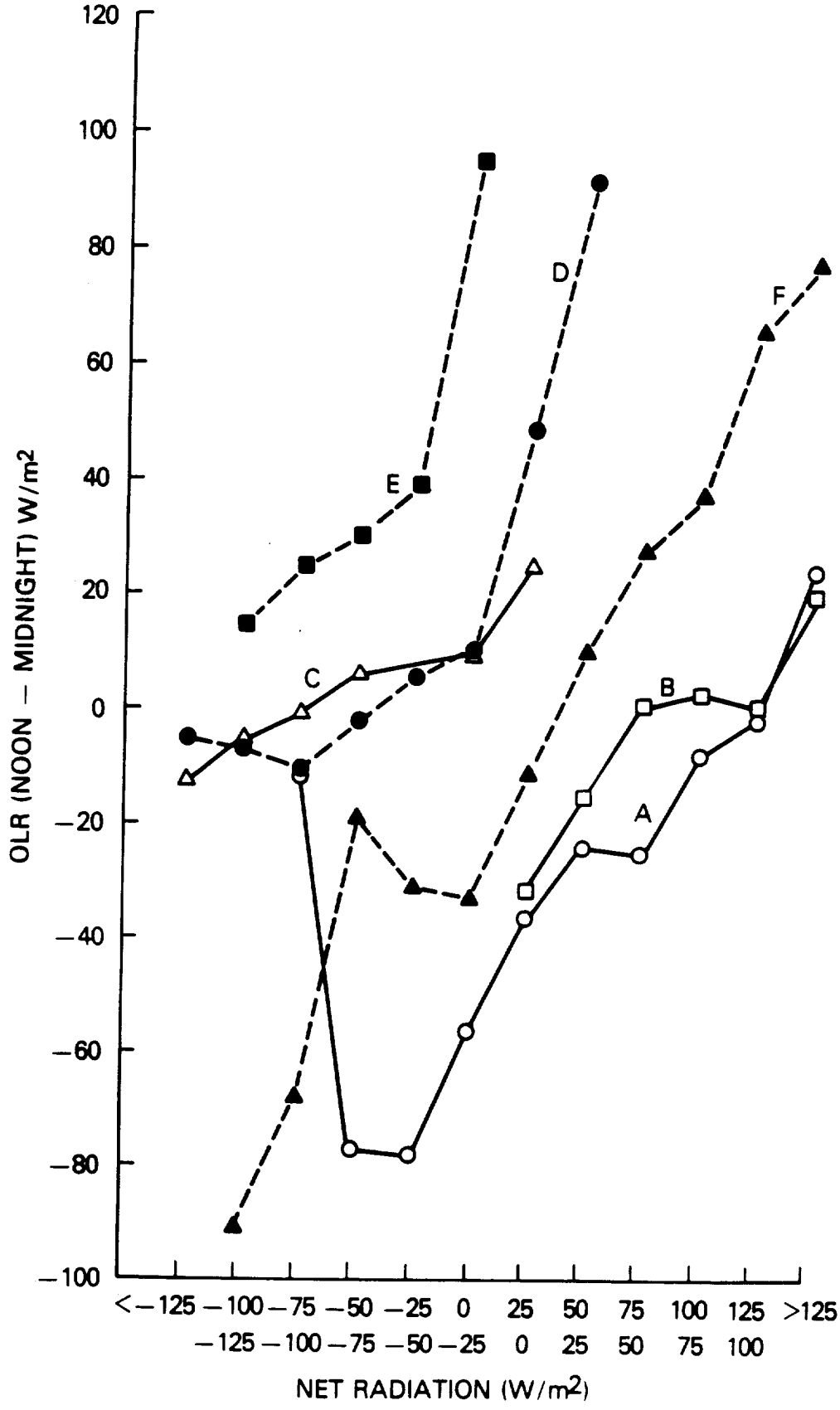

Fig. 20